**Title:** Maintenance of homeostatic plasticity at the *Drosophila* neuromuscular synapse requires continuous $IP_3$-directed signaling

**Authors and Affiliations:**

Thomas D. James [1,2], Danielle J. Zwiefelhofer [1], and C. Andrew Frank [1,3]

[1] – Department of Anatomy and Cell Biology, University of Iowa Carver College of Medicine, Iowa City, IA 52242 USA

[2] – Interdisciplinary Graduate Program in Neuroscience, University of Iowa, Iowa City, IA 52242 USA

[3] – Interdisciplinary Programs in Neuroscience, Genetics, and Molecular Medicine, University of Iowa, Iowa City, IA 52242 USA

**Address for Correspondence:** C. Andrew Frank. Department of Anatomy and Cell Biology, University of Iowa Carver College of Medicine, 51 Newton Road, 1-661A. Iowa City, IA 52242. USA.

andy-frank@uiowa.edu

## ABSTRACT

Synapses and circuits rely on neuroplasticity to adjust output and meet physiological needs. Forms of homeostatic synaptic plasticity impart stability at synapses by countering destabilizing perturbations. The *Drosophila melanogaster* larval neuromuscular junction (NMJ) is a model synapse with robust expression of homeostatic plasticity. At the NMJ, a homeostatic system detects impaired postsynaptic sensitivity to neurotransmitter and activates a retrograde signal that restores synaptic function by adjusting neurotransmitter release. This process has been separated into temporally distinct phases, induction and maintenance. One prevailing hypothesis is that a shared mechanism governs both phases. Here we show the two phases are separable. Combining genetics, pharmacology, and electrophysiology, we find that a signaling system consisting of PLCβ, inositol triphosphate ($IP_3$), $IP_3$ receptors, and Ryanodine receptors is required only for the maintenance of homeostatic plasticity. We also find that the NMJ is capable of inducing homeostatic signaling even when its sustained maintenance process is absent.

## INTRODUCTION

Synaptic plasticity is a fundamental property of neurons that underlies the activities of neuronal circuits and behaviors. Neurons have a remarkable capacity to adjust outputs in response to external cues. Depending upon context, those adjustments can be stabilizing or destabilizing to overall function. Hebbian forms of neuroplasticity are generally thought to promote destabilizing changes. A great deal is known about the molecular mechanisms underlying Hebbian paradigms of synaptic plasticity like Long Term Potentiation (LTP, e.g. (Lisman et al., 2012)) – and how Hebbian plasticity might underlie long-lasting processes like memory formation and consolidation (Andersen et al., 2017; Poo et al., 2016). Less is understood about homeostatic forms of neuroplasticity, which work to stabilize synapse function and keep activity levels within an acceptable physiological range (Davis, 2006; Davis and Müller, 2015; Delvendahl and Müller, 2019; Pozo and Goda, 2010; Turrigiano, 2017). For homeostatic plasticity, it is generally thought that coordinated actions of neurons and their targets work to maintain a set point functional parameter.

Well-studied examples of homeostatic synaptic plasticity (HSP) include synaptic scaling (O'Brien et al., 1998; Turrigiano et al., 1998; Turrigiano and Nelson, 2004), and the maintenance of evoked excitation at neuromuscular junctions (NMJs) (Cull-Candy et al., 1980; Davis and Müller, 2015; Frank, 2014a; Petersen et al., 1997). For both, the time course of implementation has been of longstanding interest. Synaptic scaling was initially shown to be a slow, chronically executed process (O'Brien et al., 1998; Turrigiano et al., 1998), but it is also possible for faster scaling mechanisms to be mobilized if multiple synaptic sites are concurrently inhibited (Sutton et al., 2006). For the NMJ, homeostatic signaling is triggered by short-term challenges to synapse function (Frank et al., 2006; Wang et al., 2016b), but it is also maintained for extended developmental time in the face of chronic challenges (Cull-Candy et al., 1980; Davis et al., 1998; DiAntonio et al., 1999; Petersen et al., 1997; Plomp et al., 1992).

The *Drosophila melanogaster* NMJ is an ideal model synapse for studying the basic question of how synapses work to counter destabilizing perturbations (Frank, 2014a). At this NMJ, reduced sensitivity to single vesicles of glutamate initiates a retrograde, muscle-to-nerve signaling

63 cascade that induces increased neurotransmitter vesicle release, or quantal content (QC). As a
64 result, the NMJ maintains a normal postsynaptic response level (Frank et al., 2006; Petersen et
65 al., 1997). Mechanistically, this increase in QC depends upon the successful execution of discrete
66 presynaptic events, such as increases in neuronal $Ca^{2+}$ influx and an increase in the size of the
67 readily releasable pool (RRP) of synaptic vesicles (Frank et al., 2006; Müller and Davis, 2012;
68 Müller et al., 2012). The field has termed this compensatory signaling process as presynaptic
69 homeostatic potentiation (PHP) (Delvendahl and Müller, 2019). Two factors that govern the ex-
70 pression of PHP are the nature of the NMJ synaptic challenge and the amount of time elapsed
71 after presentation of the challenge. Acute pharmacological inhibition of postsynaptic glutamate
72 receptors initiates a rapid induction of PHP that restores synaptic output in minutes (Frank et al.,
73 2006). By contrast, genetic lesions and other long-term reductions of NMJ sensitivity to neuro-
74 transmitter induce PHP in a way that is sustained throughout life (Brusich et al., 2015; Davis et
75 al., 1998; DiAntonio et al., 1999; Paradis et al., 2001; Petersen et al., 1997).

76 We previously identified the *Plc21C* gene as a factor needed for PHP (Brusich et al.,
77 2015). *Plc21C* encodes a *Drosophila* Phospholipase Cβ (PLCβ) homolog known to be neuronally
78 expressed (Shortridge et al., 1991) – but recent ribosomal profiling data also indicates possible
79 muscle expression of *Plc21C* (Chen and Dickman, 2017). In canonical signaling pathways, once
80 PLCβ is activated by Gαq, it cleaves the membrane lipid phosphatidylinositol 4,5-bisphosphate
81 ($PIP_2$) into diacylglycerol (DAG) and inositol triphosphate ($IP_3$). DAG can affect synaptic function
82 by activating Protein Kinase C (PKC), while $IP_3$ binds its receptor ($IP_3R$) to trigger release of cal-
83 cium from intracellular stores (Kadamur and Ross, 2012; Philip et al., 2010; Tedford and Zamponi,
84 2006). It is not understood which aspects of this signaling machinery are mobilized during PHP.
85 Potential downstream consequences of PLCβ activity at the NMJ include phosphorylation of neu-
86 ronal proteins, modulation of ion channel activity, and changes in localization of neurotransmis-
87 sion machinery (Cremona and De Camilli, 2001; Goni and Alonso, 1999; Huang et al., 2006;
88 Peters et al., 2001; Rohrbough and Broadie, 2005; Wu et al., 2002).

89 For this study, we scrutinized PLCβ-directed signaling further. We tested whether PLCβ-
90 directed signaling was required solely for the maintenance of PHP or if it could also be required
91 for induction. In addition to PLCβ, we identified the $IP_3$ Receptor (*Drosophila* Itpr, herein $IP_3R$)
92 and Ryanodine receptor (*Drosophila* RyR) as being part of the same signaling process. We found
93 that neither PLCβ, nor $IP_3R$, nor RyR are required for the rapid induction of PHP. Additionally, we
94 found that the rapid induction of PHP is still possible in synapses already sustaining PHP. Sur-
95 prisingly, we found that NMJs are capable of rapidly inducing PHP – even when the sustained
96 expression of PHP is already blocked by impairments in PLCβ, $IP_3R$, or RyR signaling. Taken
97 together, our data show that the induction and maintenance of PHP are separable. Even though
98 there is compelling evidence that parts of the induction and maintenance signaling mechanisms
99 overlap (Goel et al., 2017), it is also true that acute PHP is possible in scenarios where long-term
100 PHP is not.
101
102 **MATERIALS AND METHODS**
103
104 *Drosophila husbandry*
105 *Drosophila melanogaster* fruit flies were raised on Cornmeal, Molasses and Yeast Medium pre-
106 pared according to the Bloomington Drosophila Stock Center (BDSC, Bloomington, IN) recipe.
107 *Drosophila* husbandry was performed according to standard practices (Greenspan, 2004). Larvae
108 were raised at 25°C or 29°C in humidity controlled and light-controlled Percival DR-36VL incuba-
109 tors (Geneva Scientific).
110
111 *Drosophila genetic lines*
112 $w^{1118}$ (Hazelrigg et al., 1984) was used as a non-transgenic wild type stock. The deletion *GluRIIA*
113 allele ($GluRIIA^{SP16}$) was generated previously (Petersen et al., 1997). *UAS-$IP_3$-sponge* lines
114 (*UAS-$IP_3$-sponge.m30* and *UAS-$IP_3$-sponge.m49*) were provided by Drs. Masayuki Koganezawa
115 and Daisuke Yamamoto (Usui-Aoki et al., 2005). The *UAS-GluRIII[RNAi]* line utilized to screen

116 homeostatic candidate molecules was described previously (Brusich et al., 2015). GAL4 drivers
117 simultaneously utilized for the *"Pre- + Post-Gal4"* conditions were *elaV(C155)-Gal4* (Lin and
118 Goodman, 1994), *Sca-Gal4* (Budnik et al., 1996), and *BG57-Gal4* (Budnik et al., 1996).
119 In addition to the *UAS-IP$_3$-sponge* lines, several *UAS-RNAi* or genetic mutant lines were
120 obtained either from the BDSC or the Vienna Drosophila Resource Center (VDRC, Vienna, Aus-
121 tria). Those specific mutations and lines are detailed in Supplementary Table 2. Procedures for
122 how the *UAS-RNAi* lines were generated have been published (Dietzl et al., 2007; Ni et al., 2009).
123
124 *Electrophysiology and Pharmacology*
125 Wandering third instar larvae were collected and filleted for NMJ analysis. Control and experi-
126 mental samples were collected in parallel, using identical conditions. Activity in abdominal muscle
127 6 from segments 2 and 3 was recorded in a modified HL3 saline (70 mM NaCl, 5 mM KCl, 5 mM
128 HEPES, 10 mM NaHCO3, 115 mM sucrose, 0.5 mM $CaCl_2$ (unless otherwise noted), 10 mM
129 MgCl2, 4.2 mM trehalose, pH 7.2) (see (Stewart et al., 1994) for original parameters). Sharp elec-
130 trode recordings of miniature excitatory postsynaptic potentials (mEPSPs) and excitatory postsyn-
131 aptic potentials (EPSPs) were conducted as previously described (Brusich et al., 2015; Spring et
132 al., 2016; Yeates et al., 2017) and analyzed using MiniAnalysis (Synaptosoft) and pClamp10 (Mo-
133 lecular Devices) software, blind to genotype or treatment. Uncorrected quantal content (QC) was
134 estimated per NMJ as average EPSP/average mEPSP and was also reported as corrected for
135 non-linear summation as done previously (Martin, 1955). For the correction factor formula (Martin,
136 1955), we used a reversal potential of +10 mV (Supplemental Excel File).
137 Pharmacological agents were bath applied in recording saline at the final concentrations
138 indicated in the text, figures, and tables. The agents included Philanthotoxin-433 (PhTox, Sigma-
139 Aldrich and Santa Cruz Biotechnology), Xestospongin C (Abcam), 2-APB (Tocris, Bio-Techne
140 Corporation), Ryanodine (Tocris), and Dantrolene (Tocris).
141 To render mEPSP and EPSP traces for figures, we pulled (x,y) coordinates from the
142 Clampfit program (Molecular Devices) and imported those coordinates into GraphPad Prism

143 (GraphPad) software. For all traces, we chose a recording that was at (or closest to) the calculated
144 average. For mEPSPs, we picked a representative selection of minis. For EPSPs, the final trace
145 that was rendered was an average of all the EPSP traces from that particular NMJ.
146
147 *Immunostaining and Analyses*
148 Immunostaining and image analyses of NMJ 6/7 in segments A2 and A3 were performed as pre-
149 viously described (Spring et al., 2016; Yeates et al., 2017). Briefly, filleted larvae were fixed in
150 Bouin's fixative for 4 min, washed, incubated in primary antibodies for 2 hours, washed, and in-
151 cubated in secondary antibodies for an additional 2 hours. Bouton staining was performed to
152 assess NMJ growth by using the following primary antibodies: mouse anti-Synapsin (anti-Syn;
153 3C11) 1:50 (Developmental Studies Hybridoma Bank, Iowa City, IA) and rabbit anti-Dlg 1:15,000
154 (Budnik et al. 1996). The following fluorophore conjugated secondary antibodies were also used
155 (Jackson ImmunoResearch Laboratories): goat anti–mouse 488 1:1000 (DyLight) and goat anti–
156 rabbit 549 1:2000 (Dy-Light). Alexa-647 goat anti-HRP was utilized to stain neuronal membranes.
157 Larval preparations were mounted in Vectashield (Vector Laboratories) and imaged at room tem-
158 perature using Zen software on a Zeiss 880 Laser Scanning Microscope with an EC Plan-Neofluar
159 40X Oil DIC Objective (aperture 1.30) or an EC Plan-Apochromat 63X Oil DIC Objective (aperture
160 1.40; Zeiss). Experimental and control larval preps were imaged using identical acquisition set-
161 tings and analyzed blind to genotype using the same procedure and thresholds. Images were
162 prepared for publication in Adobe Photoshop using identical procedures for experimental and
163 control images. Anti-Dlg bouton counts were completed in a blinded fashion to quantify synapse
164 growth. For each anti-Dlg–positive bouton counted in muscle, it was verified that there was a
165 corresponding cluster of anti-Syn staining in neurons.
166
167 *Statistical Analyses*
168 For electrophysiological data, statistical significance was tested either by Student's T-Test if one
169 experimental data set was being directly compared to a control data set, or by one-way ANOVA

170 with a Bonferroni post-hoc test if multiple data sets were being compared. For bouton counting,
171 significance was tested utilizing a Kruskal-Wallis ANOVA test followed by Dunn's post-hoc test.
172 Specific *p* value ranges and tests are noted in the Figures and Figure Legends and Supplemen-
173 tary Tables and shown in graphs as follows: * $p < 0.05$, ** $p < 0.01$, and *** $p < 0.001$. All statistical
174 analyses were conducted using GraphPad Prism Software. Most figure data are plotted as violin
175 plots from GraphPad Prism; the violin plot shapes signify data distribution, *n* values are below
176 those shapes, and horizontal lines signify the $0^{th}$, $25^{th}$, $50^{th}$, $75^{th}$, and $100^{th}$ percentiles of the data.
177

178 **RESULTS**

179

180 **PLCβ loss uncouples the short-term induction of homeostatic plasticity from its long-term**
181 **maintenance**

182 Previously we demonstrated that loss-of-function of *Plc21C*, a *Drosophila melanogaster*
183 PLCβ gene, could dampen or eliminate the long-term maintenance of presynaptic homeostatic
184 potentiation (PHP) (Brusich et al., 2015). We repeated some of those experiments. We used a
185 fruit fly line containing both neuron- and muscle-GAL4 drivers as well as a *UAS-GluRIII[RNAi]*
186 transgenic construct to provide a chronic homeostatic challenge to reduce quantal size (Brusich
187 et al., 2015). *Pre-* + *Post-Gal4* >> *UAS-GluRIII[RNAi]* NMJs have decreased quantal size
188 (mEPSP, Fig. 1A) and an offsetting, homeostatic increase in quantal content (QC, Fig. 1C). This
189 increase in release keeps excitatory postsynaptic potentials (EPSPs) at control levels (Fig. 1B).
190 By contrast, concurrent knockdown of *GluRIII* and *Plc21C* gene functions by RNAi (*Pre-* + *Post-*
191 *Gal4* >> *UAS-GluRIII[RNAi]* + *Plc21C[RNAi]*) leaves this form of homeostatic potentiation only
192 partly intact (Figs. 1A-C). There is a small QC increase compared to baseline (Fig. 1C), but this
193 QC increase is blunted compared to the homeostatic challenge, resulting in evoked potentials
194 that are smaller than controls (Figs. 1B, 1D). These data are consistent with the prior results
195 (Brusich et al., 2015) (Supplementary Table S1 for summary Fig. 1 data; Raw Data Workbook for
196 raw data).

197 The *GluRIII* RNAi knock down manipulation in muscle is a days-long, chronic homeostatic
198 challenge to the maintenance of NMJ function (Brusich et al., 2015). We tested if *Plc21C* gene
199 knock down blocks or impairs the acute induction of PHP. For acute induction, we applied 20 μM
200 of the glutamate receptor antagonist Philanthotoxin-433 (PhTox) to both wild-type and to *Pre-* +
201 *Post-Gal4 >> Plc21C[RNAi]* knock down NMJs. PhTox application decreased quantal size for
202 both conditions (Fig. 1E) (Frank et al., 2006). For both conditions, evoked potentials remained
203 largely steady compared to non-PhTox controls (Figs. 1F, 1H) because there was a significant,
204 compensatory increase in quantal content (Fig. 1G). Thus, partial loss of *Plc21C* gene function is
205 not a sufficient condition to block the rapid induction of PHP.
206
207 **The induction of PHP is possible, even when PHP maintenance is impaired**
208 We used *Plc21C* loss and PhTox to test whether the capacity to maintain PHP for ex-
209 tended developmental time is required for rapid PHP induction. The most common modes of as-
210 sessing PHP at the *Drosophila* NMJ are a lifelong, genetic $GluRIIA^{SP16}$ null mutation for PHP
211 maintenance (Petersen et al., 1997) and acute PhTox application for PHP induction (Frank et al.,
212 2006). For both cases, mEPSP amplitudes are decreased and QC is increased helping to main-
213 tain evoked potentials at (or nearly at) normal levels. PhTox targets the function of GluRIIA-con-
214 taining receptors; thus, adding PhTox to a $GluRIIA^{SP16}$ null background does not further decrease
215 quantal size (Frank et al., 2006). This fact presents a difficulty in using PhTox and $GluRIIA^{SP16}$
216 together to test whether additional PHP can be acutely induced in a chronic glutamate receptor
217 loss genetic condition already sustaining PHP. We reasoned that by applying PhTox to *UAS-*
218 *GluRIII[RNAi]* knock down synapses, we could circumvent this limitation. Partial loss of the es-
219 sential subunit-encoding *GluRIII* gene leaves some GluRIIA-containing receptors intact (Brusich
220 et al., 2015). In turn, those GluRIIA-containing receptors could be subject to the secondary PhTox
221 challenge.
222 We applied PhTox to *UAS-GluRIII[RNAi]* synapses, and we observed a further decrease
223 in quantal amplitude – significantly below mEPSP size recorded for *UAS-GluRIII[RNAi]* alone (Fig.

224 1I). Evoked potentials were only slightly lower than the non-PhTox levels (slightly lower; Figs. 1J,
225 L) because there was a robust increase in QC (Fig. 1K). This result indicated that a rapid induction
226 of PHP was possible at a synapse already undergoing a sustained maintenance of PHP.

227 We next tested whether compromised ability to sustain PHP throughout life would also
228 preclude acute induction of PHP. PhTox applied to NMJs simultaneously expressing both *UAS-*
229 *GluRIII[RNAi]* and *Plc21C[RNAi]* constructs induced a significant decrease in mEPSP amplitude
230 relative to non-PhTox-treated control synapses (Fig. 1I). Yet we also observed a significant in-
231 crease in QC (i.e. PHP induction) (Fig. 1K), which kept evoked NMJ potentials similar to their non-
232 PhTox levels (Figs. 1J, L). Collectively, these data suggest that acute PHP induction does not
233 require intact PHP maintenance and that PLCβ plays a maintenance role.

234

235 **$IP_3$ function is required for the maintenance of PHP but not its induction**

236 We sought to identify potential PLCβ signaling effectors that could mediate the long-term
237 maintenance of PHP. We screened targets by electrophysiology. Based on canonical signaling
238 functions of PLCβ, we conducted a directed screen, targeting molecules such as PKC, CaMKII,
239 Unc-13, related signaling molecules, as well several potential G-protein-coupled receptors
240 (GPCRs). Additionally, we tested molecules implicated in intracellular calcium signaling, intracel-
241 lular ion channel function, and synaptic ion channel function.

242 We used a screening paradigm designed to find factors needed for the maintenance of
243 PHP: combining pre- and postsynaptic GAL4 expression with *UAS-GluRIII[RNAi]* with a tested
244 genetic manipulation (Brusich et al., 2015). We targeted factors for this screen using either *UAS-*
245 *gene* misexpression or *UAS-gene[RNAi]* constructs. We also used loss-of-function mutations. For
246 an additional screening condition for some mutations we constructed double mutant lines with a
247 $GluRIIA^{SP16}$ null deletion allele (Petersen et al., 1997). For any test, we analyzed two conditions:
248 a baseline neurotransmission condition (e.g., GAL4 + genetic manipulation alone) and a homeo-

statically challenged condition (e.g., GAL4 + genetic manipulation + *UAS-GluRIII[RNAi]*). Any homeostatically challenged condition that failed to increase QC over its own baseline condition was designated as a potential positive.

We examined 28 distinct genetic manipulations (comprising 23 distinct genes), including controls (Fig. 2A; Supplementary Table S2 for summary screen data). We plotted the relative QC values for the screen as "% baseline" (Fig. 2A), indicating how much of a QC change the *UAS-GluRIII[RNAi]* challenge yielded. We set a cutoff for a "screen positive" as a QC smaller than one standard deviation below expected the expected QC given the *UAS-GluRIII[RNAi]* homeostatic challenge (Fig. 2A, red dashed line).

Two genetic manipulations showed no statistically significant QC increase upon homeostatic challenge (Fig. 2A, red). For both manipulations, the screened target molecule was inositol 1,4,5-triphosphate ($IP_3$). $IP_3$ is a second-messenger signaling molecule. We examined it because PLCβ cleaves the phospholipid $PIP_2$ into soluble $IP_3$ and membrane-bound diacylglycerol (DAG) during canonical signaling. We targeted cellular $IP_3$ by expressing *UAS-IP$_3$-sponge*, a transgene that expresses a peptide that binds and sequesters $IP_3$ (Usui-Aoki et al., 2005). Concomitant pre- and postsynaptic expression of *UAS-IP$_3$-sponge* transgenes completely blocked the long-term expression of PHP (Figs. 2B-E). This resulted in significantly smaller EPSP amplitudes in the *UAS-GluRIII[RNAi]* PHP-challenge genetic background. (Figs. 2B, D).

We used the full block of sustained PHP by *UAS-IP$_3$-sponge* expression to re-test the relationship between the rapid induction of PHP and its long-term maintenance. First, we tested if *UAS-IP$_3$-sponge* expression alone could block the rapid induction of PHP. Following PhTox treatment, synapses expressing *UAS-IP$_3$-sponge* in pre- and postsynaptic tissues showed a significant decrease in mEPSP amplitude compared to non-PhTox controls (Fig. 2F), and yet they had steady EPSP amplitudes (Fig. 2G) because of a robust increase in QC (Fig. 2H). This result indicated that *UAS-IP$_3$-sponge* expression left the rapid induction mechanisms of PHP intact.

We next tested if the rapid induction of PHP was possible for third instar larval NMJs that had blocked PHP maintenance throughout life. To do this, we applied PhTox to NMJs expressing

276 *UAS-IP$_3$-sponge* in a *UAS-GluRIII[RNAi]* background. Even in this genetic background, we found
277 that the rapid induction of PHP remained intact following PhTox treatment (Figs. 2F-H). PhTox
278 treatment resulted in a further decrease in mEPSP amplitude compared to non-PhTox-treated
279 synapses expressing both *UAS-GluRIII[RNAi]* and *UAS-IP$_3$-sponge* (Fig. 2F), but there was an
280 offsetting increase in QC (Fig. 2H). The evoked event amplitudes were at the level of genetically
281 identical, non-PhTox treated synapses (Fig. 2G), because of successful induction of PHP in a
282 genetic background that was unable to sustain PHP throughout development.
283

284 **IP$_3$ sequestration does not impair synapse growth**

285 Chronic expression of the *UAS-IP$_3$-sponge* transgene blocked the long-term expression
286 of PHP. In principle, this result could be a secondary consequence of aberrant NMJ development.
287 To check this possibility, we co-immunostained third instar larval *Drosophila* NMJs with anti-Syn-
288 apsin (Syn, presynaptic vesicles), anti-Discs Large (Dlg, postsynaptic density), and anti-Horse-
289 radish Peroxidase (HRP, presynaptic membrane) antibodies. This allowed us to examine synaptic
290 growth by counting NMJ boutons. We quantified bouton growth for synapse 6/7, muscle segments
291 A2 and A3. We examined control conditions and conditions with blocked PHP maintenance due
292 to *UAS-IP3-sponge* expression (Figs. 3A-E). We observed no significant differences versus con-
293 trol in bouton number for any condition, for either segment A2 or A3 – including the genetic back-
294 ground where we co-expressed *UAS-IP3-sponge* and *UAS-GluRIII[RNAi]* (Fig. 3F). There were
295 also no significant differences versus control in bouton number normalized per unit muscle area
296 (Fig. 3G; Raw Data Workbook for raw bouton count and muscle size data). These data indicate
297 that when IP$_3$ is sequestered, synapse undergrowth is not causal for a PHP block.
298

299 **Pharmacology targeting IP$_3$ receptors uncouples the induction and maintenance of PHP**

300 We tested if the temporal requirements of PHP could be uncoupled by pharmacological
301 disruption of *Drosophila* IP$_3$ receptor function (Itpr in *Drosophila*). IP$_3$Rs are localized to the endo-
302 plasmic reticulum (ER) and function to mediate calcium efflux from internal stores (Berridge, 1984,

303 1987). ER is known to localize throughout neurons in *Drosophila*, including synaptic terminals
304 (Summerville et al., 2016), and recent studies have implicated ER resident proteins in the execu-
305 tion of PHP at the *Drosophila* NMJ (Genç et al., 2017; Kikuma et al., 2017). To target $IP_3Rs$, we
306 turned to two reagents known to impair function: Xestospongin C and 2-APB (2-Aminoethoxydi-
307 phenyl Borate) and applied those drugs to *GluRIIA* loss-of-function mutants.

308 Xestospongin C is a membrane-permeable drug that disrupts intracellular calcium release
309 directly via non-competitive inhibition of $IP_3Rs$ (Gafni et al., 1997; Wilcox et al., 1998). Xestospon-
310 gin C has been previously shown to inhibit *Drosophila* $IP_3Rs$ (Vazquez-Martinez et al., 2003).
311 There are caveats to its use; Xestospongin C may act indirectly by inhibiting SERCA, which could
312 lead to depletion of intracellular calcium stores (Castonguay and Robitaille, 2002). Moreover,
313 Xestospongin C has been demonstrated to impair voltage-gated $Ca^{2+}$ and $K^+$ currents in guinea
314 pig smooth muscle (Ozaki et al., 2002). In principle, these latter activities on intact fly NMJ tissue
315 could impact baseline neurotransmission parameters (Bergquist et al., 2010; Brusich et al., 2015;
316 Jan et al., 1977; Peng and Wu, 2007).

317 *GluRIIA*$^{SP16}$ null mutant NMJs have a marked decrease in quantal size (Fig. 4A) (Petersen
318 et al., 1997). This homozygous null condition does not perfectly maintain control EPSP amplitudes
319 (Fig. 4B) (Brusich et al., 2015; Frank et al., 2006; Frank et al., 2009; Spring et al., 2016; Yeates
320 et al., 2017). However, the null does induce a robust increase in QC, which signifies a long-term
321 implementation of PHP (Fig. 4C). *GluRIIA*$^{SP16}$ NMJ preparations acutely treated with 20 μM Xes-
322 tospongin C (10 minutes) displayed an expected decrease in mEPSP amplitude compared to
323 non-*GluRIIA*$^{SP16}$ controls (Fig. 4A). However, these drug-treated NMJs failed to show an increase
324 in QC (Fig. 4C). This resulted in markedly decreased evoked amplitudes (Figs. 4B, G). Thus, not
325 only did 20 μM Xestospongin C induce a block of PHP maintenance, but it was capable of extin-
326 guishing this long-term maintenance process on a timescale of minutes.

327 Importantly, 20 μM Xestospongin C did not impair baseline neurotransmission in a wild-
328 type background (Figs. 4B, G); this suggests that 20 μM Xestospongin C does not impair the
329 function of other important voltage-gated channels at the *Drosophila* NMJ. Finally, in the *GluRIIA*

330 null background, neither a lower dose (5 μM Xestospongin C) nor vehicle application alone inhib-
331 ited the expression of PHP (Figs. 4A-C) (Supplementary Table S3 for summary Fig. 4 data; Raw
332 Data Workbook for raw data).

333 Next, we tested if acute application of 20 μM Xestospongin C could block the rapid induc-
334 tion of PHP. We applied 20 μM Xestospongin C to wild-type NMJs concurrently with 20 μM PhTox.
335 Quantal size was markedly diminished compared to the non-PhTox control (Fig. 4D; vehicle con-
336 trol dataset same as in 4A-C). Yet evoked amplitudes remained near control levels (Figs. 4E, G)
337 because the rapid induction of PHP was intact (Fig. 4F).

338 We used 2-APB as a second reagent to target $IP_3Rs$. 2-APB is a membrane-permeable
339 drug that has variable effects. It is known to impair $IP_3R$ (Diver et al., 2001; Maruyama et al.,
340 1997). There are also reports that 2-APB can impair targets such as Transient Receptor Potential
341 (TRP) channels (Bootman et al., 2002; Xu et al., 2005). If continuous $IP_3R$ function were required
342 for the maintenance PHP at NMJs, we reasoned that acute application of 2-APB (as with Xes-
343 tospongin C) should also extinguish this form of neuroplasticity.

344 We applied both 1 μM and 10 μM 2-APB to *GluRIIA*$^{SP16}$ null NMJs. Both drug concentra-
345 tions resulted in a failure to increase QC compared to drug-treated wild-type controls; this resulted
346 in small evoked events for the drug-treated *GluRIIA*$^{SP16}$ NMJs because PHP maintenance was
347 blocked (Figs. 5A-C, G) (Supplementary Table S4 for summary Fig. 5 data; Raw Data Workbook
348 for raw data). Next, we tested if 2-APB blocks the PhTox-induced rapid induction of PHP. We
349 applied 1 μM 2-APB concurrently with 20 μM PhTox. Evoked potentials remained near the level
350 of 2-APB-treated NMJs without PhTox (Figs. 5E, H) because 1 μM 2-APB left the rapid induction
351 of PHP intact (Figs. 5D-F).

352 We note that 2-APB potentiated baseline neurotransmission, seemingly in a dose-depend-
353 ent way (Figs. 5B, G). This potentiation likely means that 2-APB had off-target effects at the NMJ
354 in addition to $IP_3Rs$. We considered that 2-APB could exert effects though TRP channels, like
355 Drosophila Inactive (Iav). Iav plays a role in NMJ neurotransmission and controls $Ca^{2+}$ levels in
356 motor neurons (Wong et al., 2014). However, knock down of *iav* gene function by RNAi did not

357 impair PHP in our screen (Supplementary Table S2), and the effects of 2-APB on baseline neu-
358 rotransmission appear to be the opposite of those reported for strong *iav* loss of function (Wong
359 et al., 2014). Taken together, our pharmacological data show that with acute drug application of
360 either Xestospongin C or 2-APB, it is acutely possible to erase a lifelong, *GluRIIA*$^{SP16}$-induced
361 long-term expression of PHP. Since this erasure is accomplished with known inhibitors of $IP_3R$,
362 our data are consistent with the hypothesis that the maintenance of PHP requires continuous $IP_3R$
363 function.
364

365 **Pharmacology targeting Ryanodine Receptors uncouples the induction and maintenance**
366 **of PHP**

367 Ryanodine receptors (RyRs) also mediate release of calcium from ER stores (Berridge,
368 1998; Simkus and Stricker, 2002). RyRs are localized to the ER in excitable tissues like neurons
369 and muscle (Santulli and Marks, 2015; Santulli et al., 2017). Therefore, we tested whether RyRs
370 are also required for the maintenance of PHP at the NMJ. We repeated the same types of exper-
371 iments executed with the $IP_3R$ pharmacological blockade – this time targeting *Drosophila* RyRs
372 by utilizing Ryanodine (Murmu et al., 2010) and Dantrolene (Vazquez-Martinez et al., 2003; Zhao
373 et al., 2001) at concentrations previously reported to block RyRs. We acquired similar results as
374 with $IP_3R$ blockade. Acute application of either 100 μM Ryanodine or 10 μM Dantrolene to *GluRIIA*
375 null preparations resulted in failure of PHP maintenance. QC did not increase for the homeostat-
376 ically challenged condition (*GluRIIA* + drug) versus the unchallenged condition (wild-type + drug)
377 (Figs. 6A-C) (Supplementary Table S5 for summary Fig. 6 data; Raw Data Workbook for raw
378 data).

379 Next, we tested whether RyR inhibition could block the rapid induction of PHP. As was the
380 case with $IP_3R$ inhibition, acute application of 10 μM Dantrolene to PhTox-treated NMJs did not
381 disrupt the short-term induction of PHP (Figs. 6D-F). We extended our analysis by re-examining
382 the condition where we combined a long-term homeostatic challenge (*GluRIII[RNAi]*) with a short-
383 term challenge (PhTox) to further decrease quantal size (as in Figs. 1I-L). In this double-challenge

384 condition, addition of 10 μM Dantrolene left the rapid induction portion of PHP intact (Figs. 6D-G).
385 Collectively, these experiments demonstrate that acute pharmacological perturbations targeting
386 RyRs are capable of uncoupling the short-term induction and the long-term maintenance of PHP.
387

388 **Dual $IP_3$ sequestration and RyR blockade are not additive**

389 In some tissues, RyR is activated by $IP_3R$-mediated $Ca^{2+}$ release, in a signaling process
390 termed Calcium-Induced Calcium Release (CICR) (Berridge, 1998). $IP_3Rs$ and RyRs have been
391 placed together in CICR signaling processes in other systems, and our group has also identified
392 overlapping functions of $IP_3R$ and RyR at the NMJ (Brusich et al., 2018). Thus, we tested if $IP_3$
393 signaling and RyR functions might support the maintenance of PHP at the *Drosophila* NMJ via a
394 shared process. The expectation for a shared process would be that a dual block of PHP (con-
395 sisting of $IP_3$ sequestration + RyR pharmacological blockade) would not depress evoked trans-
396 mission or quantal content below either individual manipulation.

397 A chronic *GluRIII[RNAi]*-expression NMJ challenge is amenable both to pharmacology
398 and dual-tissue *UAS-IP$_3$-sponge* expression (*Pre-* + *Post-Gal4*). In the *GluRIII[RNAi]* genetic
399 background, both 10 μM Dantrolene application and *UAS-IP$_3$-sponge* expression blocked the
400 long-term maintenance of PHP (Figs. 7A-C). This resulted in EPSPs that were blunted compared
401 to *GluRIII[RNAi]*-alone controls (Figs. 7B, D). When we combined Dantrolene application and
402 *UAS-IP$_3$-sponge* expression in the *GluRIII[RNAi]* background, the PHP impairment was indistin-
403 guishable from the impairment elicited by Dantrolene alone or *UAS-IP$_3$-sponge* alone (Figs. 7A-
404 D) (Supplementary Table S6 for summary Fig. 7 data; Raw Data Workbook for raw data). The
405 data are consistent with a model in which $IP_3$ sequestration and RyR blockade disrupt the long-
406 term maintenance of PHP as part of a shared process, either via a single linear pathway or con-
407 vergent pathways.
408

409 **Axotomy does not block rapid PHP, even when $IP_3$ signaling is impaired**

410 For larval NMJ electrophysiology, motor neurons are severed several minutes before re-
411 cording (Jan and Jan, 1976). Although standard practice, this procedure requires special attention
412 in our study because store-operated calcium release mediates a variety of cellular responses
413 after axotomy in rodent (Rigaud et al., 2009) and nematode models (Sun et al., 2014). For the
414 rapid induction of PHP at the NMJ, PhTox is typically applied to intact synapses, prior to motor
415 nerve severing and recording (Frank et al., 2006). This allows for endogenous spontaneous ac-
416 tivity to drive PhTox to bind to open channels prior to recording (Frank et al., 2006). Nevertheless,
417 rapid induction of PHP still works effectively when the motor nerves are severed prior to PhTox
418 exposure (Frank et al., 2006).

419 To test for a possible synergistic interaction between axotomy, $IP_3$-directed signaling, and
420 ER function during the acute induction phase of PHP, we applied PhTox to NMJs with intact motor
421 nerves or with cut motor nerves (central nervous system (CNS) excised). We did this in a genetic
422 background while expressing *UAS-IP$_3$-sponge* construct pre- and postsynaptically. For controls,
423 we treated the preparations identically and used GAL4 drivers alone for the genetic background.
424 We found that rapid PHP induction still worked in the *UAS-IP$_3$-sponge*-expressing background,
425 regardless of whether the motor nerve was severed prior to PhTox application (Figs. 7E-G). The
426 evoked events were slightly diminished for the *UAS-IP$_3$-sponge* expressing NMJs where the CNS
427 was cut out of the preparation prior to PhTox application (Figs. 7F, H). However, by quantal con-
428 tent measures, the rapid induction of PHP was not blocked by this dual treatment (Fig. 7G).

429

430 **Neuron and muscle $IP_3$ signaling both contribute to long-term homeostatic potentiation**

431 Insofar, none of the genetic or pharmacological manipulations impairing PHP maintenance
432 in this study have been tissue specific. In principle, all PHP-blocking manipulations described
433 could operate either in neuronal or muscle substrates – or upon both tissues. Our prior work
434 showed that chronic *Plc21C* gene knockdown in the muscle alone is not sufficient to impair PHP
435 (Brusich et al., 2015). That result suggested a neuronal component to this signaling system for
436 PHP maintenance. Yet further tests are needed. We wished to understand whether a pre- or

437 postsynaptic mechanism (or a dual-tissue mechanism) governs $IP_3$-mediated $Ca^{2+}$ store release
438 signaling in order to support long-term maintenance of PHP.

439 We turned again to the *UAS-IP$_3$-sponge* transgene because it can be expressed in a tis-
440 sue-specific manner, and it conveyed a full block of PHP when dually expressed in the neuron
441 and muscle (Fig. 2). We expressed *UAS-IP$_3$-sponge* in a GAL4 driver (neuron or muscle alone)
442 or a driver + *GluRIIA$^{SP16}$* null genetic background. We then quantified PHP by NMJ electrophysi-
443 ology, considering neuronal (Figs. 8A-C) or muscle (Figs. 8D-F) expression (Supplementary Ta-
444 ble S7 for summary Fig. 8 data; Raw Data Workbook for raw data). Surprisingly, we did not local-
445 ize the full block of PHP maintenance to a single tissue. For expression in either tissue alone,
446 there was still a small increase in QC in a *Gal4 >> UAS-IP$_3$-sponge* + *GluRIIA$^{SP16}$* genetic condi-
447 tion, compared to control *Gal4 >> UAS-IP$_3$-sponge* expression in an unchallenged background
448 (Figs. 8C, F). EPSP values were depressed when *UAS-IP$_3$-sponge* was expressed neuronally in
449 the *GluRIIA* null background (Figs. 8B, G), consistent with an important neuronal component to
450 PHP (Brusich et al., 2015). Combined with our prior data (Fig. 2), we conclude that the mainte-
451 nance of PHP can be fully erased by $IP_3$ sequestration – but only if this is done in a dual tissue
452 manner.

453 Our data indicate that $IP_3$ functions in a shared process with $Ca^{2+}$ store release. Presyn-
454 aptic neurotransmitter release at the NMJ and other synapses is highly sensitive to changes in
455 intracellular $Ca^{2+}$ concentration after influx through voltage-gated $Ca_V2$ channels. Therefore, we
456 checked if $IP_3$ signaling and its effects on intracellular $Ca^{2+}$ release might impinge upon the $Ca^{2+}$
457 sensing machinery in the presynaptic cleft, which could potentially influence PHP. We conducted
458 NMJ recordings over a range of low extracellular [$Ca^{2+}$] and calculated the $Ca^{2+}$ cooperativity of
459 release for the dual-tissue expression *UAS-IP$_3$-sponge* NMJs, as well as wild-type NMJs and
460 GAL4 driver control NMJs. The $Ca^{2+}$ cooperativity of release was steady between the three con-
461 ditions (Fig. 8H, I), indicating that sequestration of cellular $IP_3$ at the NMJ does not directly alter
462 the $Ca^{2+}$-dependence of synaptic release at the presynaptic NMJ.

463 **DISCUSSION**

464 In this study, we divided the acute induction and chronic maintenance stages of presyn-
465 aptic homeostatic potentiation. Our data support two core findings. The first is that the short-term
466 induction and long-term maintenance of PHP are separable by genetic and pharmacological ma-
467 nipulations. The second is that an $IP_3$-mediated signaling system is specifically required for the
468 maintenance of PHP (Fig. 9).

469

470 **Acute Versus Chronic PHP Expression**

471 For several years, one assumption has been that both the acute and chronic forms of PHP
472 are executed in a similar way – and possibly by shared mechanisms. The issue has been clouded
473 by the fact that both PhTox and a *GluRIIA* deletion mutant – the primary reagents utilized to induce
474 PHP – have the same molecular target, i.e. GluRIIA-containing glutamate receptors (Frank et al.,
475 2006; Petersen et al., 1997). The process of combining these acute and chronic forms of plasticity
476 within a single genotypic background was cumbersome due to a lack of reagents available to
477 conduct temporally separate targeting experiments.

478 Several groups ascertained insights into temporal requirements by targeting potential ho-
479 meostatic signaling genes. The main finding has been that the majority of molecules identified are
480 essential to both the acute and chronic forms of PHP (Davis and Müller, 2015; Frank, 2014a).
481 Neurons tightly control neurotransmitter release probability, and the core presynaptic machinery
482 directly responsible for increasing quantal content is shared. These shared components include
483 the $Ca_V2$-type voltage-gated calcium channel or factors gating influx through the channel (Frank
484 et al., 2006; Frank et al., 2009; Müller and Davis, 2012; Wang et al., 2014; Wang et al., 2016a;
485 Younger et al., 2013). They also include factors that regulate the size of the readily releasable
486 pool (RRP) of presynaptic vesicles (Harris et al., 2015; Müller et al., 2015; Müller et al., 2012;
487 Wang et al., 2016a; Wentzel et al., 2018; Weyhersmüller et al., 2011) or factors that control the
488 baseline excitability of the presynaptic motor neuron (Bergquist et al., 2010; Orr et al., 2017b;

489 Parrish et al., 2014; Younger et al., 2013) – and neurotransmitter fusion events themselves (Dick-
490 man and Davis, 2009; Dickman et al., 2012; Müller et al., 2011). As a result, both the acute and
491 chronic forms of PHP signaling cause increases in readily releasable pool (RRP) size and $Ca_V2$-
492 mediated calcium influx; and in turn, these presynaptic mechanisms underlie the increases in QC
493 which constitute PHP (Davis and Müller, 2015; Müller and Davis, 2012; Müller et al., 2012).

494 Here we show that although the acute and chronic processes might overlap, they are
495 functionally separable. The fact that they are separable is not necessarily surprising. This finding
496 mirrors data for discrete molecules required for long-term PHP maintenance, such as Target of
497 Rapamycin (TOR) (Goel et al., 2017; Kauwe et al., 2016; Penney et al., 2012), the Rho-type
498 guanine exchange factor Ephexin (Frank et al., 2009), the transcription factor Gooseberry (Marie
499 et al., 2010), C-terminal Src Kinase (Spring et al., 2016), innate immune signals molecules IMD,
500 IKKβ, Relish (Harris et al., 2018) and the kinesin adaptor Arl8 (Goel et al., 2019; Vukoja et al.,
501 2018). Importantly, this list contains molecules implicated both in neuron and muscle. We have
502 added PLCβ (Brusich et al., 2015) and its effectors $IP_3R$ and RyR to this list.

503 Recent studies have augmented the idea of overlapping signaling pathways and added a
504 degree of specificity. Both acute and chronic forms of PHP begin as instructive retrograde signals
505 in the muscle (Orr et al., 2017a), involve decrease in phosphorylation of muscle CaMKII levels,
506 and converge upon the same signaling components in the presynaptic neuron (Goel et al., 2017;
507 Li et al., 2018; Newman et al., 2017). These studies suggest that Tor converges on the same
508 molecular targets as acute forms of PHP (Goel et al., 2017). However, the precise roles for Tor
509 and CaMKII in either form of PHP are as yet unknown.

510 Our data appear to contradict the idea of PHP pathway convergence (Goel et al., 2017).
511 Yet our findings are not incompatible with this idea. Multiple lines of evidence indicate discrete
512 signaling requirements for acute forms of PHP on both sides of the synapse. A convergence point
513 is undefined. Accounting for the separation of acute and chronic forms of PHP – as well as their
514 discrete signaling requirements – long-term maintenance of PHP might integrate multiple signals

515 between the muscle and neuron over time. For future studies, it will be important to clearly define
516 roles of signaling systems underlying PHP and how distinct signaling systems might be linked.

517 **Unexpected findings about PHP stage separation**

518 Our work presents unexpected findings. The first is that even in the face of a chronic im-
519 pairment or block of homeostatic potentiation, the NMJ is nevertheless capable of a full rapid
520 induction of PHP (Figs. 1, 2, 7). Given that most molecules required for PHP identified to date are
521 needed for both phases, we did not expect significant functional separation between them. We
522 expected *a priori* that a failure of the chronic maintenance of PHP would make core machinery
523 unavailable for its acute induction. The second unexpected finding is how quickly the chronic
524 maintenance of PHP can be nullified by pharmacology (10 min), resulting in a return to baseline
525 neurotransmitter release probability after only minutes of drug exposure (Figs. 4-6). We showed
526 that homeostatic potentiation in *GluRIIA* mutant larvae or *GluRIII* knock-down larvae was abro-
527 gated by four different reagents previously known to block $IP_3R$ (Figs. 4, 5) or RyR (Fig. 6). Those
528 findings are reminiscent of prior work showing that acute blockade of DAG/ENaC channels with
529 the drug benzamil abolishes PHP in both a *GluRIIA* mutant background, as well as in the presence
530 of PhTox (Younger et al., 2013). A difference between benzamil application and the pharmaco-
531 logical agents used in our study is that the drugs we employed only abolished PHP in a chronically
532 challenged background.

533

534 **Does PHP induction lead to maintenance?**

535 It is unclear how signaling systems that drive homeostatic plasticity transition from a state
536 of induction to a state of maintenance. It is also not understood how interdependent short-term
537 and long-term HSP implementation mechanisms are. A more complete understanding of the tim-
538 ing and perdurance of these properties could have important implications for neurological condi-
539 tions where synapse stability is episodically lost (Russell et al., 2013).

540 Our findings parallel recent data examining active zone protein intensities in the contexts
541 of induction of PHP and maintenance of PHP at the NMJ. There are multiple results informative

542 to our study. First, the expression of any form of PHP (acute or chronic) appears to correlate with
543 an increased intensity of active zone protein levels, such as $Ca_V2$/Cacophony (Gratz et al., 2019),
544 UNC-13 (Böhme et al., 2019), and the Drosophila CAST/ELKS homolog Bruchpilot (Böhme et al.,
545 2019; Goel et al., 2019; Gratz et al., 2019). Unexpectedly, however, two of these studies also
546 reported that the rapid induction of PHP does not require this protein increase in order to be
547 functionally executed (Böhme et al., 2019; Goel et al., 2019). These are conundrums for future
548 work. How does rapid active zone remodeling happen in minutes on a mechanistic level? In the
549 absence of such remodeling, how PHP is still able to be induced rapidly? Moreover, is the ob-
550 served short-term active zone remodeling the kernel for the longer-term changes to the active
551 zone and release probability – or is some other signaling system triggered over long periods of
552 developmental time?

553 Our findings add a new dimension to those puzzles with the data that $IP_3$ signaling is
554 continuously required to maintain PHP. If active zone remodeling truly is instructive for PHP
555 maintenance, then it will be interesting to test what roles $IP_3$ signaling and intracellular calcium
556 release play in that process. Our screen did include a *UAS-RNAi* line against *unc-13* and an
557 upstream GPCR-encoding gene *methuselah* (Supplementary Table S2). Moreover, we previously
558 published a study of PHP using a *UAS-cac[RNAi]* line (Brusich et al., 2015). Chronic PHP mainte-
559 nance was intact for all of those manipulations. Those findings are not necessarily contradictory
560 to the recent work from other groups. For instance, knockdown of an active zone protein by RNAi
561 is not a null condition. As such, RNAi-mediated knockdown should leave residual wild-type protein
562 around. In theory, that residual protein could be scaled with homeostatic need.

563

564 **PLCβ- and $IP_3$-directed Signaling is Required for PHP Maintenance**

565 Our data strongly suggest that intracellular calcium channel activation and store release
566 fine tune neurotransmitter release that is implemented by PHP. The exact mechanism by which
567 $IP_3R$ and RyR function to maintain PHP at the NMJ is unclear. It appears to be a shared process
568 with $IP_3$ (Fig. 7). If these store-release channels are acting downstream of $IP_3$ activity, then our

569 data suggest that this would be a coordinated activity involving both the muscle and the neuron
570 (Figs. 8, 9) – with loss of $IP_3$ signaling in the neuron being more detrimental to evoked release
571 (Fig. 8G).

572 It remains unclear what signals are acting upstream. PLCβ is canonically activated by Gαq
573 signaling. From our prior work, we garnered evidence that a *Drosophila* Gq protein plays a role in
574 the long-term maintenance of HSP (Brusich et al., 2015). Logically, there may exist a G-protein
575 Coupled Receptor (GPCR) that functions upstream of PLCβ/$IP_3$ signaling. Our screen did not
576 positively identify such a GPCR. We did examine several genes encoding GPCRs, including
577 *TkR86C*, *mAChR-A*, *GABA-B-R1*, *PK2-R2*, *methuselah*, *AdoR*, and *mGluR* (Supplementary Ta-
578 ble S2). We also examined genes encoding Gβ subunits or putative scaffolding molecules, in-
579 cluding *CG7611* (a WD40-repeat-encoding gene), *Gβ13F*, and *Gβ76C*, again with no positive
580 screen hits (Supplementary Table S2).

581 Our data are consistent with dual pre- and postsynaptic functions of $IP_3$. This could mean
582 dual pre- and postsynaptic roles for calcium store release – through an undetermined combination
583 of RyR and $IP_3R$ activities, again either pre- or postsynaptic. Both RyR and $IP_3R$ have been shown
584 to be critical for specific aspects of neuroplasticity and neurotransmission (Berridge, 2016). Activ-
585 ities of both RyR and $IP_3R$ can activate molecules that drive plasticity, such as Calcineurin (Victor
586 et al., 1995) and CaMKII (Shakiryanova et al., 2011). At rodent hippocampal synapses, electro-
587 physiological measures like paired-pulse facilitation and frequency of spontaneous neurotrans-
588 mitter release (Emptage et al., 2001) are modulated by RyR and/or $IP_3R$ function, as is facilitation
589 of evoked neurotransmitter at the rat neocortex (Mathew and Hablitz, 2008). In addition to vesicle
590 fusion apparatus, activity of presynaptic voltage gated calcium channels is modulated by intracel-
591 lular calcium (Catterall, 2011; Lee et al., 2000). Our own work at the NMJ has shown that impairing
592 factors needed for store-operated calcium release can mollify hyperexcitability phenotypes
593 caused by gain-of-function $Ca_V2$ amino-acid substitutions (Brusich et al., 2018).

594 Within the presynaptic neuron, $IP_3R$ and RyR could activate any number of calcium-de-
595 pendent molecules to propagate homeostatic signaling. We tested some candidates in our screen

596 (Fig. 2, Supplementary Table S2), but none of those tests blocked PHP. One possibility is that
597 the reagents we utilized did not sufficiently diminish the function of target molecules enough to
598 impact PHP in this directed screen. Detection of downstream effectors specific to muscle or neu-
599 ron might also be hampered by the fact that attenuation of $IP_3$ signaling in a single tissue is insuf-
600 ficient to abrogate PHP. Another possibility is that presynaptic store calcium efflux via $IP_3R$ and
601 RyR may directly potentiate neurotransmitter release, either by potentiating basal calcium levels
602 or synchronously with $Ca_V2$-type voltage gated calcium channels (Frank et al., 2006; Müller and
603 Davis, 2012).

604 Both pre- and postsynaptic voltage-gated calcium channels are critical for the expression
605 of several forms of homeostatic synaptic plasticity (Frank, 2014b). Much evidence supports the
606 hypothesis that store-operated channels and voltage gated calcium channels interact to facilitate
607 PHP. In various neuronal populations, both RyR and $IP_3R$ interact with L-type calcium channels
608 physically and functionally to reciprocally impact the opening of the other channel (Chavis et al.,
609 1996; Kim et al., 2007; Ouardouz et al., 2003). In presynaptic boutons, RyR calcium release fol-
610 lows action potential firing (Emptage et al., 2001). Calcium imaging experiments show that both
611 the acute expression and sustained maintenance of PHP requires an increase in presynaptic
612 calcium following an action potential (Müller and Davis, 2012). Because $IP_3Rs$ are activated by
613 both free calcium and $IP_3$, elevated $IP_3$ levels in the case of chronically expressed PHP could
614 allow $IP_3Rs$ and RyRs to open in a way that is time-locked with $Ca_V2$-mediated calcium influx or
615 in a way to facilitate the results of later $Ca_V2$-mediated influx.

616

617 **ACKNOWLEDGEMENTS**

618 We thank members of the Frank lab for helpful comments on earlier versions of this study, and
619 the laboratories of Drs. Tina Tootle, Fang Lin, Toshihiro Kitamoto, Pamela Geyer, and Lori
620 Wallrath for helpful discussions. We also thank Drs. Andrew Russo, N. Charles Harata, and Chris-
621 topher Ahern for helpful suggestions. We thank the Bloomington Drosophila Stock Center and the

622 Vienna Drosophila Resource Center for several fly stocks detailed in the Materials and Methods
623 Section and Supplementary Tables.

624 **REFERENCES**

625


626 Andersen, N., Krauth, N., and Nabavi, S. (2017). Hebbian plasticity in vivo: relevance and
627 induction. Curr Opin Neurobiol *45*, 188-192.

628 Bergquist, S., Dickman, D.K., and Davis, G.W. (2010). A hierarchy of cell intrinsic and target-
629 derived homeostatic signaling. Neuron *66*, 220-234.

630 Berridge, M.J. (1984). Inositol trisphosphate and diacylglycerol as second messengers.
631 Biochem J *220*, 345-360.

632 Berridge, M.J. (1987). Inositol trisphosphate and diacylglycerol: two interacting second
633 messengers. Annu Rev Biochem *56*, 159-193.

634 Berridge, M.J. (1998). Neuronal calcium signaling. Neuron *21*, 13-26.

635 Berridge, M.J. (2016). The Inositol Trisphosphate/Calcium Signaling Pathway in Health and
636 Disease. Physiol Rev *96*, 1261-1296.

637 Böhme, M.A., McCarthy, A.W., Grasskamp, A.T., Beuschel, C.B., Goel, P., Jusyte, M., Laber,
638 D., Huang, S., Rey, U., Petzoldt, A.G.*, et al.* (2019). Rapid active zone remodeling consolidates
639 presynaptic potentiation. Nat Commun *10*, 1085.

640 Bootman, M.D., Collins, T.J., Mackenzie, L., Roderick, H.L., Berridge, M.J., and Peppiatt, C.M.
641 (2002). 2-aminoethoxydiphenyl borate (2-APB) is a reliable blocker of store-operated Ca2+
642 entry but an inconsistent inhibitor of InsP3-induced Ca2+ release. FASEB journal : official
643 publication of the Federation of American Societies for Experimental Biology *16*, 1145-1150.

644 Brusich, D.J., Spring, A.M., and Frank, C.A. (2015). A single-cross, RNA interference-based
645 genetic tool for examining the long-term maintenance of homeostatic plasticity. Frontiers in
646 cellular neuroscience *9*, 107.

647 Brusich, D.J., Spring, A.M., James, T.D., Yeates, C.J., Helms, T.H., and Frank, C.A. (2018).
648 Drosophila CaV2 channels harboring human migraine mutations cause synapse
649 hyperexcitability that can be suppressed by inhibition of a Ca2+ store release pathway. PLoS
650 genetics *14*, e1007577.

651 Budnik, V., Koh, Y.H., Guan, B., Hartmann, B., Hough, C., Woods, D., and Gorczyca, M. (1996).
652 Regulation of synapse structure and function by the Drosophila tumor suppressor gene dlg.
653 Neuron *17*, 627-640.

654 Castonguay, A., and Robitaille, R. (2002). Xestospongin C is a potent inhibitor of SERCA at a
655 vertebrate synapse. Cell Calcium *32*, 39-47.

656 Catterall, W.A. (2011). Voltage-gated calcium channels. Cold Spring Harb Perspect Biol *3*,
657 a003947.

658 Chavis, P., Fagni, L., Lansman, J.B., and Bockaert, J. (1996). Functional coupling between
659 ryanodine receptors and L-type calcium channels in neurons. Nature *382*, 719-722.

660 Chen, X., and Dickman, D. (2017). Development of a tissue-specific ribosome profiling
661 approach in Drosophila enables genome-wide evaluation of translational adaptations. PLoS
662 genetics *13*, e1007117.

663 Cremona, O., and De Camilli, P. (2001). Phosphoinositides in membrane traffic at the synapse.
664 Journal of cell science *114*, 1041-1052.

665 Cull-Candy, S.G., Miledi, R., Trautmann, A., and Uchitel, O.D. (1980). On the release of
666 transmitter at normal, myasthenia gravis and myasthenic syndrome affected human end-plates.
667 J Physiol *299*, 621-638.

668 Davis, G.W. (2006). Homeostatic control of neural activity: from phenomenology to molecular
669 design. Annu Rev Neurosci *29*, 307-323.

670 Davis, G.W., DiAntonio, A., Petersen, S.A., and Goodman, C.S. (1998). Postsynaptic PKA
671 controls quantal size and reveals a retrograde signal that regulates presynaptic transmitter
672 release in Drosophila. Neuron *20*, 305-315.

673 Davis, G.W., and Müller, M. (2015). Homeostatic control of presynaptic neurotransmitter
674 release. Annu Rev Physiol *77*, 251-270.

675 Delvendahl, I., and Müller, M. (2019). Homeostatic plasticity-a presynaptic perspective. Curr
676 Opin Neurobiol *54*, 155-162.

677 DiAntonio, A., Petersen, S.A., Heckmann, M., and Goodman, C.S. (1999). Glutamate receptor
678 expression regulates quantal size and quantal content at the Drosophila neuromuscular
679 junction. J Neurosci *19*, 3023-3032.

680 Dickman, D.K., and Davis, G.W. (2009). The schizophrenia susceptibility gene dysbindin
681 controls synaptic homeostasis. Science *326*, 1127-1130.

682 Dickman, D.K., Tong, A., and Davis, G.W. (2012). Snapin is critical for presynaptic homeostatic
683 plasticity. J Neurosci *32*, 8716-8724.

684 Dietzl, G., Chen, D., Schnorrer, F., Su, K.C., Barinova, Y., Fellner, M., Gasser, B., Kinsey, K.,
685 Oppel, S., Scheiblauer, S.*, et al.* (2007). A genome-wide transgenic RNAi library for conditional
686 gene inactivation in Drosophila. Nature *448*, 151-156.

687 Diver, J.M., Sage, S.O., and Rosado, J.A. (2001). The inositol trisphosphate receptor antagonist
688 2-aminoethoxydiphenylborate (2-APB) blocks Ca2+ entry channels in human platelets: cautions
689 for its use in studying Ca2+ influx. Cell calcium *30*, 323-329.

690 Emptage, N.J., Reid, C.A., and Fine, A. (2001). Calcium stores in hippocampal synaptic boutons
691 mediate short-term plasticity, store-operated Ca2+ entry, and spontaneous transmitter release.
692 Neuron *29*, 197-208.

693 Frank, C.A. (2014a). Homeostatic plasticity at the Drosophila neuromuscular junction.
694 Neuropharmacology *78*, 63-74.

695 Frank, C.A. (2014b). How voltage-gated calcium channels gate forms of homeostatic synaptic
696 plasticity. Frontiers in cellular neuroscience *8*, 40.

697 Frank, C.A., Kennedy, M.J., Goold, C.P., Marek, K.W., and Davis, G.W. (2006). Mechanisms
698 underlying the rapid induction and sustained expression of synaptic homeostasis. Neuron *52*,
699 663-677.

700 Frank, C.A., Pielage, J., and Davis, G.W. (2009). A presynaptic homeostatic signaling system
701 composed of the Eph receptor, ephexin, Cdc42, and CaV2.1 calcium channels. Neuron *61*, 556-
702 569.

703 Gafni, J., Munsch, J.A., Lam, T.H., Catlin, M.C., Costa, L.G., Molinski, T.F., and Pessah, I.N.
704 (1997). Xestospongins: potent membrane permeable blockers of the inositol 1,4,5-trisphosphate
705 receptor. Neuron *19*, 723-733.

706 Genç, Ö., Dickman, D.K., Ma, W., Tong, A., Fetter, R.D., and Davis, G.W. (2017). MCTP is an
707 ER-resident calcium sensor that stabilizes synaptic transmission and homeostatic plasticity.
708 eLife *6*.

709 Goel, P., Dufour Bergeron, D., Bohme, M.A., Nunnelly, L., Lehmann, M., Buser, C., Walter,
710 A.M., Sigrist, S.J., and Dickman, D. (2019). Homeostatic scaling of active zone scaffolds
711 maintains global synaptic strength. J Cell Biol.

712 Goel, P., Li, X., and Dickman, D. (2017). Disparate Postsynaptic Induction Mechanisms
713 Ultimately Converge to Drive the Retrograde Enhancement of Presynaptic Efficacy. Cell reports
714 *21*, 2339-2347.

715 Goni, F.M., and Alonso, A. (1999). Structure and functional properties of diacylglycerols in
716 membranes. Progress in lipid research *38*, 1-48.

717 Gratz, S.J., Goel, P., Bruckner, J.J., Hernandez, R.X., Khateeb, K., Macleod, G.T., Dickman, D.,
718 and O'Connor-Giles, K.M. (2019). Endogenous Tagging Reveals Differential Regulation of
719 Ca(2+) Channels at Single Active Zones during Presynaptic Homeostatic Potentiation and
720 Depression. J Neurosci *39*, 2416-2429.

721 Greenspan, R.J. (2004). Fly pushing : the theory and practice of Drosophila genetics, 2nd edn
722 (Cold Spring Harbor, N.Y.: Cold Spring Harbor Laboratory Press).

723 Harris, N., Braiser, D.J., Dickman, D.K., Fetter, R.D., Tong, A., and Davis, G.W. (2015). The
724 Innate Immune Receptor PGRP-LC Controls Presynaptic Homeostatic Plasticity. Neuron *88*,
725 1157-1164.

726 Harris, N., Fetter, R.D., Brasier, D.J., Tong, A., and Davis, G.W. (2018). Molecular Interface of
727 Neuronal Innate Immunity, Synaptic Vesicle Stabilization, and Presynaptic Homeostatic
728 Plasticity. Neuron *100*, 1163-1179 e1164.

729 Hazelrigg, T., Levis, R., and Rubin, G.M. (1984). Transformation of white locus DNA in
730 drosophila: dosage compensation, zeste interaction, and position effects. Cell *36*, 469-481.

731 Huang, F.D., Woodruff, E., Mohrmann, R., and Broadie, K. (2006). Rolling blackout is required
732 for synaptic vesicle exocytosis. J Neurosci *26*, 2369-2379.

733 Jan, L.Y., and Jan, Y.N. (1976). Properties of the larval neuromuscular junction in Drosophila
734 melanogaster. J Physiol *262*, 189-214.

735 Jan, Y.N., Jan, L.Y., and Dennis, M.J. (1977). Two mutations of synaptic transmission in
736 Drosophila. Proc R Soc Lond B Biol Sci *198*, 87-108.

737 Kadamur, G., and Ross, E.M. (2012). Mammalian Phospholipase C. Annu Rev Physiol.

738 Kauwe, G., Tsurudome, K., Penney, J., Mori, M., Gray, L., Calderon, M.R., Elazouzzi, F.,
739 Chicoine, N., Sonenberg, N., and Haghighi, A.P. (2016). Acute Fasting Regulates Retrograde
740 Synaptic Enhancement through a 4E-BP-Dependent Mechanism. Neuron *92*, 1204-1212.

741 Kikuma, K., Li, X., Kim, D., Sutter, D., and Dickman, D.K. (2017). Extended Synaptotagmin
742 Localizes to Presynaptic ER and Promotes Neurotransmission and Synaptic Growth in
743 Drosophila. Genetics.

744 Kim, S., Yun, H.M., Baik, J.H., Chung, K.C., Nah, S.Y., and Rhim, H. (2007). Functional
745 interaction of neuronal Cav1.3 L-type calcium channel with ryanodine receptor type 2 in the rat
746 hippocampus. The Journal of biological chemistry *282*, 32877-32889.

747 Lee, A., Scheuer, T., and Catterall, W.A. (2000). Ca2+/calmodulin-dependent facilitation and
748 inactivation of P/Q-type Ca2+ channels. J Neurosci *20*, 6830-6838.

749 Li, X., Goel, P., Chen, C., Angajala, V., Chen, X., and Dickman, D.K. (2018). Synapse-specific
750 and compartmentalized expression of presynaptic homeostatic potentiation. eLife *7*.

751 Lin, D.M., and Goodman, C.S. (1994). Ectopic and increased expression of Fasciclin II alters
752 motoneuron growth cone guidance. Neuron *13*, 507-523.

753 Lisman, J., Yasuda, R., and Raghavachari, S. (2012). Mechanisms of CaMKII action in long-
754 term potentiation. Nat Rev Neurosci *13*, 169-182.

755 Marie, B., Pym, E., Bergquist, S., and Davis, G.W. (2010). Synaptic homeostasis is consolidated
756 by the cell fate gene gooseberry, a Drosophila pax3/7 homolog. J Neurosci *30*, 8071-8082.

757 Martin, A.R. (1955). A further study of the statistical composition on the end-plate potential. J
758 Physiol *130*, 114-122.

759 Maruyama, T., Kanaji, T., Nakade, S., Kanno, T., and Mikoshiba, K. (1997). 2APB, 2-
760 aminoethoxydiphenyl borate, a membrane-penetrable modulator of Ins(1,4,5)P3-induced Ca2+
761 release. J Biochem *122*, 498-505.

762 Mathew, S.S., and Hablitz, J.J. (2008). Calcium release via activation of presynaptic IP3
763 receptors contributes to kainate-induced IPSC facilitation in rat neocortex. Neuropharmacology
764 *55*, 106-116.

765 Müller, M., and Davis, G.W. (2012). Transsynaptic control of presynaptic Ca(2)(+) influx
766 achieves homeostatic potentiation of neurotransmitter release. Curr Biol *22*, 1102-1108.

767 Müller, M., Genç, Ö., and Davis, G.W. (2015). RIM-Binding Protein Links Synaptic Homeostasis
768 to the Stabilization and Replenishment of High Release Probability Vesicles. Neuron *85*, 1056-
769 1069.

770 Müller, M., Liu, K.S., Sigrist, S.J., and Davis, G.W. (2012). RIM Controls Homeostatic Plasticity
771 through Modulation of the Readily-Releasable Vesicle Pool. J Neurosci *32*, 16574-16585.

772 Müller, M., Pym, E.C., Tong, A., and Davis, G.W. (2011). Rab3-GAP controls the progression of
773 synaptic homeostasis at a late stage of vesicle release. Neuron *69*, 749-762.

774 Murmu, M.S., Stinnakre, J., and Martin, J.R. (2010). Presynaptic Ca2+ stores contribute to odor-
775 induced responses in Drosophila olfactory receptor neurons. J Exp Biol *213*, 4163-4173.

776 Newman, Z.L., Hoagland, A., Aghi, K., Worden, K., Levy, S.L., Son, J.H., Lee, L.P., and Isacoff,
777 E.Y. (2017). Input-Specific Plasticity and Homeostasis at the Drosophila Larval Neuromuscular
778 Junction. Neuron *93*, 1388-1404 e1310.

779 Ni, J.Q., Liu, L.P., Binari, R., Hardy, R., Shim, H.S., Cavallaro, A., Booker, M., Pfeiffer, B.D.,
780 Markstein, M., Wang, H.*, et al.* (2009). A Drosophila resource of transgenic RNAi lines for
781 neurogenetics. Genetics *182*, 1089-1100.

782 O'Brien, R.J., Kamboj, S., Ehlers, M.D., Rosen, K.R., Fischbach, G.D., and Huganir, R.L.
783 (1998). Activity-dependent modulation of synaptic AMPA receptor accumulation. Neuron *21*,
784 1067-1078.

785 Orr, B.O., Fetter, R.D., and Davis, G.W. (2017a). Retrograde semaphorin-plexin signalling
786 drives homeostatic synaptic plasticity. Nature *550*, 109-113.

787 Orr, B.O., Gorczyca, D., Younger, M.A., Jan, L.Y., Jan, Y.N., and Davis, G.W. (2017b).
788 Composition and Control of a Deg/ENaC Channel during Presynaptic Homeostatic Plasticity.
789 Cell reports *20*, 1855-1866.

790 Ouardouz, M., Nikolaeva, M.A., Coderre, E., Zamponi, G.W., McRory, J.E., Trapp, B.D., Yin, X.,
791 Wang, W., Woulfe, J., and Stys, P.K. (2003). Depolarization-induced Ca2+ release in ischemic
792 spinal cord white matter involves L-type Ca2+ channel activation of ryanodine receptors.
793 Neuron *40*, 53-63.

794 Ozaki, H., Hori, M., Kim, Y.S., Kwon, S.C., Ahn, D.S., Nakazawa, H., Kobayashi, M., and
795 Karaki, H. (2002). Inhibitory mechanism of xestospongin-C on contraction and ion channels in
796 the intestinal smooth muscle. Br J Pharmacol *137*, 1207-1212.

797 Paradis, S., Sweeney, S.T., and Davis, G.W. (2001). Homeostatic control of presynaptic release
798 is triggered by postsynaptic membrane depolarization. Neuron *30*, 737-749.

799 Parrish, J.Z., Kim, C.C., Tang, L., Bergquist, S., Wang, T., Derisi, J.L., Jan, L.Y., Jan, Y.N., and
800 Davis, G.W. (2014). Kruppel mediates the selective rebalancing of ion channel expression.
801 Neuron *82*, 537-544.

802 Peng, I.F., and Wu, C.F. (2007). Drosophila cacophony channels: a major mediator of neuronal
803 Ca2+ currents and a trigger for K+ channel homeostatic regulation. J Neurosci *27*, 1072-1081.

804 Penney, J., Tsurudome, K., Liao, E.H., Elazzouzi, F., Livingstone, M., Gonzalez, M., Sonenberg,
805 N., and Haghighi, A.P. (2012). TOR is required for the retrograde regulation of synaptic
806 homeostasis at the Drosophila neuromuscular junction. Neuron *74*, 166-178.

807 Peters, C., Bayer, M.J., Buhler, S., Andersen, J.S., Mann, M., and Mayer, A. (2001). Trans-
808 complex formation by proteolipid channels in the terminal phase of membrane fusion. Nature
809 *409*, 581-588.

810 Petersen, S.A., Fetter, R.D., Noordermeer, J.N., Goodman, C.S., and DiAntonio, A. (1997).
811 Genetic analysis of glutamate receptors in Drosophila reveals a retrograde signal regulating
812 presynaptic transmitter release. Neuron *19*, 1237-1248.

813 Philip, F., Kadamur, G., Silos, R.G., Woodson, J., and Ross, E.M. (2010). Synergistic activation
814 of phospholipase C-beta3 by Galpha(q) and Gbetagamma describes a simple two-state
815 coincidence detector. Curr Biol *20*, 1327-1335.

816 Plomp, J.J., van Kempen, G.T., and Molenaar, P.C. (1992). Adaptation of quantal content to
817 decreased postsynaptic sensitivity at single endplates in alpha-bungarotoxin-treated rats. J
818 Physiol *458*, 487-499.

819 Poo, M.M., Pignatelli, M., Ryan, T.J., Tonegawa, S., Bonhoeffer, T., Martin, K.C., Rudenko, A.,
820 Tsai, L.H., Tsien, R.W., Fishell, G.*, et al.* (2016). What is memory? The present state of the
821 engram. BMC Biol *14*, 40.

822 Pozo, K., and Goda, Y. (2010). Unraveling mechanisms of homeostatic synaptic plasticity.
823 Neuron *66*, 337-351.

824 Rigaud, M., Gemes, G., Weyker, P.D., Cruikshank, J.M., Kawano, T., Wu, H.E., and Hogan,
825 Q.H. (2009). Axotomy depletes intracellular calcium stores in primary sensory neurons.
826 Anesthesiology *111*, 381-392.

827 Rohrbough, J., and Broadie, K. (2005). Lipid regulation of the synaptic vesicle cycle. Nat Rev
828 Neurosci *6*, 139-150.

829 Russell, J.F., Fu, Y.H., and Ptacek, L.J. (2013). Episodic neurologic disorders: syndromes,
830 genes, and mechanisms. Annu Rev Neurosci *36*, 25-50.

831 Santulli, G., and Marks, A.R. (2015). Essential Roles of Intracellular Calcium Release Channels
832 in Muscle, Brain, Metabolism, and Aging. Curr Mol Pharmacol *8*, 206-222.

833 Santulli, G., Nakashima, R., Yuan, Q., and Marks, A.R. (2017). Intracellular calcium release
834 channels: an update. J Physiol *595*, 3041-3051.

835 Shakiryanova, D., Morimoto, T., Zhou, C., Chouhan, A.K., Sigrist, S.J., Nose, A., Macleod, G.T.,
836 Deitcher, D.L., and Levitan, E.S. (2011). Differential control of presynaptic CaMKII activation
837 and translocation to active zones. The Journal of neuroscience : the official journal of the
838 Society for Neuroscience *31*, 9093-9100.

839 Shortridge, R.D., Yoon, J., Lending, C.R., Bloomquist, B.T., Perdew, M.H., and Pak, W.L.
840 (1991). A Drosophila phospholipase C gene that is expressed in the central nervous system. J
841 Biol Chem *266*, 12474-12480.

842 Simkus, C.R., and Stricker, C. (2002). The contribution of intracellular calcium stores to
843 mEPSCs recorded in layer II neurones of rat barrel cortex. J Physiol *545*, 521-535.

844 Spring, A.M., Brusich, D.J., and Frank, C.A. (2016). C-terminal Src Kinase Gates Homeostatic
845 Synaptic Plasticity and Regulates Fasciclin II Expression at the Drosophila Neuromuscular
846 Junction. PLoS genetics *12*, e1005886.

847 Stewart, B.A., Atwood, H.L., Renger, J.J., Wang, J., and Wu, C.F. (1994). Improved stability of
848 Drosophila larval neuromuscular preparations in haemolymph-like physiological solutions.
849 Journal of comparative physiology A, Sensory, neural, and behavioral physiology *175*, 179-191.

850 Summerville, J.B., Faust, J.F., Fan, E., Pendin, D., Daga, A., Formella, J., Stern, M., and
851 McNew, J.A. (2016). The effects of ER morphology on synaptic structure and function in
852 Drosophila melanogaster. Journal of cell science *129*, 1635-1648.

853 Sun, L., Shay, J., McLoed, M., Roodhouse, K., Chung, S.H., Clark, C.M., Pirri, J.K., Alkema,
854 M.J., and Gabel, C.V. (2014). Neuronal regeneration in C. elegans requires subcellular calcium
855 release by ryanodine receptor channels and can be enhanced by optogenetic stimulation. J
856 Neurosci *34*, 15947-15956.

857 Sutton, M.A., Ito, H.T., Cressy, P., Kempf, C., Woo, J.C., and Schuman, E.M. (2006). Miniature
858 neurotransmission stabilizes synaptic function via tonic suppression of local dendritic protein
859 synthesis. Cell *125*, 785-799.

860 Tedford, H.W., and Zamponi, G.W. (2006). Direct G protein modulation of Cav2 calcium
861 channels. Pharmacol Rev *58*, 837-862.

862 Turrigiano, G.G. (2017). The dialectic of Hebb and homeostasis. Philos Trans R Soc Lond B
863 Biol Sci *372*.

864 Turrigiano, G.G., Leslie, K.R., Desai, N.S., Rutherford, L.C., and Nelson, S.B. (1998). Activity-
865 dependent scaling of quantal amplitude in neocortical neurons. Nature *391*, 892-896.

866 Turrigiano, G.G., and Nelson, S.B. (2004). Homeostatic plasticity in the developing nervous
867 system. Nat Rev Neurosci *5*, 97-107.

868 Usui-Aoki, K., Matsumoto, K., Koganezawa, M., Kohatsu, S., Isono, K., Matsubayashi, H.,
869 Yamamoto, M.T., Ueda, R., Takahashi, K., Saigo, K.*, et al.* (2005). Targeted expression of Ip3
870 sponge and Ip3 dsRNA impaires sugar taste sensation in Drosophila. Journal of neurogenetics
871 *19*, 123-141.

872 Vazquez-Martinez, O., Canedo-Merino, R., Diaz-Munoz, M., and Riesgo-Escovar, J.R. (2003).
873 Biochemical characterization, distribution and phylogenetic analysis of Drosophila melanogaster
874 ryanodine and IP3 receptors, and thapsigargin-sensitive Ca2+ ATPase. Journal of cell science
875 *116*, 2483-2494.

876 Victor, R.G., Thomas, G.D., Marban, E., and O'Rourke, B. (1995). Presynaptic modulation of
877 cortical synaptic activity by calcineurin. Proceedings of the National Academy of Sciences of the
878 United States of America *92*, 6269-6273.

879 Vukoja, A., Rey, U., Petzoldt, A.G., Ott, C., Vollweiter, D., Quentin, C., Puchkov, D., Reynolds,
880 E., Lehmann, M., Hohensee, S.*, et al.* (2018). Presynaptic Biogenesis Requires Axonal
881 Transport of Lysosome-Related Vesicles. Neuron *99*, 1216-1232 e1217.

882 Wang, T., Hauswirth, A.G., Tong, A., Dickman, D.K., and Davis, G.W. (2014). Endostatin Is a
883 Trans-Synaptic Signal for Homeostatic Synaptic Plasticity. Neuron *83*, 616-629.

884 Wang, T., Jones, R.T., Whippen, J.M., and Davis, G.W. (2016a). alpha2delta-3 Is Required for
885 Rapid Transsynaptic Homeostatic Signaling. Cell reports *16*, 2875-2888.

886 Wang, X., Pinter, M.J., and Rich, M.M. (2016b). Reversible Recruitment of a Homeostatic
887 Reserve Pool of Synaptic Vesicles Underlies Rapid Homeostatic Plasticity of Quantal Content. J
888 Neurosci *36*, 828-836.

889 Wentzel, C., Delvendahl, I., Sydlik, S., Georgiev, O., and Müller, M. (2018). Dysbindin links
890 presynaptic proteasome function to homeostatic recruitment of low release probability vesicles.
891 Nat Commun *9*, 267.

892 Weyhersmüller, A., Hallermann, S., Wagner, N., and Eilers, J. (2011). Rapid active zone
893 remodeling during synaptic plasticity. J Neurosci *31*, 6041-6052.

894 Wilcox, R.A., Primrose, W.U., Nahorski, S.R., and Challiss, R.A. (1998). New developments in
895 the molecular pharmacology of the myo-inositol 1,4,5-trisphosphate receptor. Trends Pharmacol
896 Sci *19*, 467-475.

897 Wong, C.O., Chen, K., Lin, Y.Q., Chao, Y., Duraine, L., Lu, Z., Yoon, W.H., Sullivan, J.M.,
898 Broadhead, G.T., Sumner, C.J.*, et al.* (2014). A TRPV channel in Drosophila motor neurons
899 regulates presynaptic resting Ca2+ levels, synapse growth, and synaptic transmission. Neuron
900 *84*, 764-777.

901 Wu, L., Bauer, C.S., Zhen, X.G., Xie, C., and Yang, J. (2002). Dual regulation of voltage-gated
902 calcium channels by PtdIns(4,5)P2. Nature *419*, 947-952.

903 Xu, S.Z., Zeng, F., Boulay, G., Grimm, C., Harteneck, C., and Beech, D.J. (2005). Block of
904 TRPC5 channels by 2-aminoethoxydiphenyl borate: a differential, extracellular and voltage-
905 dependent effect. Br J Pharmacol *145*, 405-414.

906 Yeates, C.J., Zwiefelhofer, D.J., and Frank, C.A. (2017). The Maintenance of Synaptic
907 Homeostasis at the Drosophila Neuromuscular Junction Is Reversible and Sensitive to High
908 Temperature. eNeuro *4*.

909 Younger, M.A., Müller, M., Tong, A., Pym, E.C., and Davis, G.W. (2013). A presynaptic ENaC
910 channel drives homeostatic plasticity. Neuron *79*, 1183-1196.

911 Zhao, F., Li, P., Chen, S.R., Louis, C.F., and Fruen, B.R. (2001). Dantrolene inhibition of
912 ryanodine receptor Ca2+ release channels. Molecular mechanism and isoform selectivity. The
913 Journal of biological chemistry *276*, 13810-13816.

914

915

## FIGURE AND TABLE LEGENDS

**Figure 1: Maintenance of presynaptic homeostatic potentiation requires PLCβ, but induction does not.**

**(A)** *GluRIII* knockdown induces a significant decrease in quantal size for both driver control and *Plc21C* knockdown genetic backgrounds. **(B)** EPSP amplitudes are maintained with *GluRIII* knockdown alone but dampened with concurrent *GluRIII* and *Plc21C* knockdown. **(C)** There is significant PHP (Presynaptic Homeostatic Potentiation, measured as an increase in quantal content) in response to *GluRIII* knockdown. **(D)** Representative electrophysiological traces of EPSPs (above) and mEPSPs (below). The evoked events show full PHP in the *GluRIII* RNAi knock down background and partial PHP with concurrent *Plc21C* knock down. **(E)** 10-minute incubation with 20 μM PhTox diminishes quantal size for all conditions. **(F)** EPSP amplitudes after acute PhTox incubation are maintained at or near normal levels. **(G)** The data in (F) are because PHP is rapidly induced in wild-type and *Plc21C* RNAi NMJs after PhTox incubation. **(H)** Representative electrophysiological traces show fully intact PHP induction. **(I)** With dual PHP maintenance (GluRIII knockdown) and induction (PhTox application), quantal size is further decreased. **(J)** EPSP amplitudes after dual maintenance and induction. **(K)** Quantal is content further increased in by PhTox treatment in *GluRIII* RNAi synapses compared to untreated synapses; this expression of PHP does not require full PLCβ function. **(L)** Representative electrophysiological traces illustrate that even though PHP maintenance is impaired with PLCβ knockdown, PHP induction is not impaired. Violin plots have horizontal lines signifying the $0^{th}$, $25^{th}$, $50^{th}$, $75^{th}$, and $100^{th}$ percentiles of the data distribution; the distribution itself is delineated by the shapes of the plots. * $p < 0.05$, ** $p < 0.01$, *** $p < 0.001$ by Student's T-Test versus non-challenged genetic control or by one-way ANOVA with a Bonferroni post-hoc test in the case of comparing degree of compensation with *GluRIII* RNAi and *Plc21C* RNAi + *GluRIII* RNAi. Scale bars for all traces are $y$ = 10 mV (1 mV), $x$ = 20 ms (500 ms) for EPSPs (mEPSPs).

**Figure 2: $IP_3$ sequestration blocks PHP maintenance but not PHP induction.**

**(A)** Screen data, plotting baseline quantal content (QC, $x$-axis, genetic manipulation alone) versus QC of the homeostatically challenged condition ($y$-axis, *GluRIII RNAi* or *GluRIIA* mutant). Blue = *GluRIIA* alone. Green = *GluRIII* RNAi alone. Red = *GluRIII RNAi* + *UAS-$IP_3$-sponge.* Dotted line = one standard deviation below the mean QC of *GluRIII* RNAi. **(B)** Representative electrophysiological traces (EPSPs above; mEPSPs below), demonstrating diminished evoked potentials in the

952 *GluRIII RNAi* + *UAS-IP$_3$-sponge* (presynaptic + postsynaptic expression) condition. **(C)** *GluRIII*
953 knockdown induces a significant decrease in quantal size for all genetic backgrounds. **(D)** EPSP
954 amplitudes are maintained with *GluRIII* knockdown alone but significantly diminished with con-
955 current *GluRIII* knockdown and expression of either *UAS-IP$_3$-sponge line*. **(E)** By quantal content,
956 sustained PHP expression is abolished when *UAS-IP$_3$-sponge* is expressed using concurrent pre-
957 and postsynaptic GAL4 drivers. **(F)** 10-minute incubation with 20 μM PhTox diminishes quantal
958 size for all conditions. **(G)** EPSP amplitudes after acute PhTox incubation are maintained at or
959 near normal levels for all conditions. **(H)** Failure to sustain PHP following $IP_3$ sequestration does
960 not preclude its rapid induction. The data in (G) are because PhTox treatment results in a com-
961 pensatory increase in QC for conditions shown. **(I)** Representative electrophysiological traces
962 showing full homeostatic compensation with PhTox application (as in (Frank et al., 2006)). **(J)**
963 Representative traces of the experimental data in (F-H). Violin plots used as in Fig. 1. * $p < 0.05$,
964 ** $p < 0.01$, *** $p < 0.001$ by Student's T-Test versus non-challenged genetic control. Scale bars
965 for all traces are $y$ = 10 mV (1 mV), $x$ = 20 ms (500 ms) for EPSPs (mEPSPs).
966
967
968 **Figure 3: $IP_3$ sequestration does not impair NMJ growth**
969
970 **(A-E)** NMJs were co-stained with anti-DLG (red) and anti-Synapsin antibodies (green) to visualize
971 synaptic boutons, with anti-HRP (blue) to visualize presynaptic membranes. Genotypes or condi-
972 tions as indicated. All scale bars, 10 μm. **(F)** NMJ growth was assessed by bouton counting at
973 abdominal segments A2 and A3, muscle 6/7, based on postsynaptic DLG staining and double
974 checked for presynaptic Synapsin. No statistically significant differences in NMJ growth versus
975 driver control were observed for any of the experimental conditions ($p > 0.1$ vs. control, regardless
976 of segment). **(G)** Bouton counts were normalized per unit of muscle 6/7 area. No statistically sig-
977 nificant differences versus control were observed ($p > 0.2$ vs. control, regardless of segment).
978 Violin plots used as in Fig. 1. For both F and G, data were compared for each segment individually
979 using the Kruskal-Wallis ANOVA test followed by Dunn's multiple comparisons test.
980
981 **Figure 4: Xestospongin C blocks PHP maintenance but not PHP induction.**
982
983 Xestospongin C acutely applied to NMJs to impair $IP_3R$ function. **(A)** The *GluRIIA$^{SP16}$* deletion
984 mutation diminishes quantal size for all experimental conditions. **(B)** EPSP amplitudes are some-
985 what impaired versus non-*GluRIIA* control in all cases but most severely impaired when *GluRIIA*
986 deletion is combined with 20 μM Xestospongin C incubation. **(C)** By quantal content, sustained

987 PHP expression is abolished with acute NMJ exposure to 20 μM Xestospongin C. **(D)** Acute in-
988 cubation 20 μM PhTox diminishes quantal size for all conditions (PhTox + DMSO vehicle or PhTox
989 + 20 μM Xestospongin C). **(E)** EPSP amplitudes are normal or near normal for all conditions. **(F)**
990 Rapid PHP induction by PhTox not blocked by 20 μM Xestospongin C. **(G)** Representative elec-
991 trophysiological traces (EPSPs above; mEPSPs below) for 20 μM Xestospongin C (or control)
992 conditions in (A-F). Violin plots used as in Fig. 1. * $p < 0.05$, ** $p < 0.01$, *** $p < 0.001$ by Student's
993 T-Test versus non-challenged genetic control. Scale bars for all traces are $y$ = 10 mV (1 mV), $x$ =
994 20 ms (500 ms) for EPSPs (mEPSPs).
995
996 **Figure 5: 2-APB blocks PHP maintenance but not PHP induction.**
997
998 2-APB acutely applied to NMJs to impair $IP_3R$ function. Wild-type and *GluRIIA* control data sets
999 are replotted from Figure 4 for visual comparison. **(A)** The *GluRIIA*$^{SP16}$ deletion mutation dimin-
1000 ishes quantal size for all experimental conditions. **(B)** EPSP amplitudes are somewhat impaired
1001 versus non-*GluRIIA* control in all cases but severely impaired when *GluRIIA* deletion is combined
1002 with either 1 μM or 10 μM 2-APB incubation. **(C)** By quantal content, sustained PHP expression
1003 is abolished with acute NMJ exposure to 1 μM or 10 μM 2-APB. **(D)** Acute incubation 20 μM
1004 PhTox diminishes quantal size for all conditions (PhTox + DMSO vehicle or PhTox + 1 μM 2-
1005 APB). **(E)** EPSP amplitudes are normal or near normal for all conditions. **(F)** Rapid PHP induction
1006 by PhTox not blocked by 1 μM 2-APB. **(G)** Representative electrophysiological traces (EPSPs
1007 above; mEPSPs below) for 10 μM 2-APB (or control) conditions in (A-C). **(H)** Representative
1008 electrophysiological traces for 1 μM 2-APB (or control) conditions in (D-F). Violin plots used as in
1009 Fig. 1. * $p < 0.05$, ** $p < 0.01$, *** $p < 0.001$ by Student's T-Test versus non-challenged genetic
1010 control. Scale bars in (G) also apply to (H) and are $y$ = 10 mV (1 mV), $x$ = 20 ms (500 ms) for
1011 EPSPs (mEPSPs).
1012
1013 **Figure 6: The maintenance of PHP requires continuous RyR function, but PHP induction**
1014 **does not.**
1015
1016 Ryanodine or Dantrolene acutely applied to NMJs to impair RyR function. Wild-type and *GluRIIA*
1017 control data sets are replotted from Figures 4 and 5 for visual comparison. **(A)** The *GluRIIA*$^{SP16}$
1018 deletion mutation diminishes quantal size for all experimental conditions. **(B)** EPSP amplitudes
1019 are somewhat impaired versus non-*GluRIIA* control in all cases but most severely impaired when
1020 *GluRIIA* deletion is combined with 10 μM Dantrolene. **(C)** By quantal content, sustained PHP
1021 expression is abolished with acute NMJ exposure to 100 μM Ryanodine or 10 μM Dantrolene. **(D)**

1022 Acute incubation 20 μM PhTox diminishes quantal size for all conditions shown. **(E)** EPSP ampli-
1023 tudes remain near genetic control levels for all conditions with PhTox application. **(F)** Rapid PHP
1024 induction by PhTox is intact in the presence of 10 μM Dantrolene, even when *GluRIII* has been
1025 knocked down throughout life. **(G)** Representative electrophysiological traces for the conditions
1026 in (D-F). Violin plots used as in Fig. 1. Statistical comparisons are by Student's T-Test vs. unchal-
1027 lenged controls. * $p < 0.05$, ** $p < 0.01$, *** $p < 0.001$. Scale bars for all traces are $y$ = 10 mV (1
1028 mV), $x$ = 20 ms (500 ms) for EPSPs (mEPSPs).
1029
1030 **Figure 7: There are no additive effects of genetic $IP_3$ signaling inhibition and pharmacolog-**
1031 **ical RyR inhibition. (A)** *GluRIII* knockdown diminishes quantal size for all experimental condi-
1032 tions. **(B)** When challenged with *GluRIII* knockdown, EPSP amplitudes are maintained for the
1033 GAL4 driver control background but impaired for all other experimental backgrounds. The dual
1034 manipulation of 10 μM Dantrolene + *UAS-$IP_3$-sponge* is indistinguishable from the single manip-
1035 ulations alone. **(C)** By quantal content, sustained PHP expression is abolished with chronic IP3
1036 sequestration, acute 10 μM Dantrolene application, or both. **(D)** Representative electrophysiolog-
1037 ical traces for the conditions in (A-C). **(E)** Acute incubation 20 μM PhTox diminishes quantal size
1038 for all conditions shown. **(F)** EPSP amplitudes remain near genetic control levels for all conditions
1039 with PhTox application. There is a slight diminishment for the condition in which *UAS-$IP_3$-sponge*
1040 is expressed and PhTox application is performed only after nerve dissection. **(G)** Full, rapid PHP
1041 induction or partial PHP induction by PhTox is present for all conditions shown. **(H)** Representa-
1042 tive electrophysiological traces for the conditions in (E-G). Violin plots used as in Fig. 1. Statistical
1043 comparisons for (A-C) and for wild type vs. wild type + PhTox are by Student's T-Test vs. unchal-
1044 lenged controls. Statistical comparisons across three data sets are by one-way ANOVA followed
1045 by Bonferroni post-hoc test across genotypes shown. * $p < 0.05$, ** $p < 0.01$, *** $p < 0.001$. Scale
1046 bars for all traces are $y$ = 10 mV (1 mV), $x$ = 20 ms (500 ms) for EPSPs (mEPSPs).
1047
1048 **Figure 8: Combined pre-and postsynaptic $IP_3$ signaling maintains PHP.** *UAS-$IP_3$-sponge*
1049 transgene expression in single tissue types impairs PHP maintenance, but does not block it. *$IP_3$-*
1050 *sponge* either in neurons (A-C) or muscle (D-F). Wild-type and *GluRIIA* control data sets are
1051 replotted from Figures 4-6 for visual comparison. **(A)** The *GluRIIA$^{SP16}$* deletion mutation dimin-
1052 ishes quantal size for all experimental conditions. **(B)** EPSP amplitudes are somewhat impaired
1053 versus non-*GluRIIA* control in all cases but most severely impaired when *GluRIIA* deletion is com-
1054 bined with presynaptic *$IP_3$-sponge* expression. **(C)** By quantal content, sustained PHP is still pre-
1055 sent for all conditions shown. **(D)** The *GluRIIA$^{SP16}$* deletion mutation diminishes quantal size for
1056 all experimental conditions. **(E)** EPSP amplitudes are somewhat impaired versus non-*GluRIIA*

control. **(F)** By quantal content, sustained PHP is still present for all conditions shown. **(G)** Representative electrophysiological traces for conditions in (A-F). **(H)** *UAS-IP$_3$-sponge* transgene expression does not impair calcium cooperativity of release. **(I)** Representative electrophysiological trances for conditions in (H). Violin plots used as in Fig. 1. Statistical comparisons are by one-way ANOVA followed by Bonferroni post-hoc test across genotypes shown. * $p < 0.05$, ** $p < 0.01$, *** $p < 0.001$. Scale bars in (G) apply to all traces in (G) and (I) and are $y$ = 10 mV (1 mV), $x$ = 20 ms (500 ms) for EPSPs (mEPSPs).

**Figure 9. Model depicting PLCβ/IP3R/RyR signaling underling the maintenance of PHP in both muscle and neuron.** At the *Drosophila* NMJ, PLCβ and effectors IP$_3$R and RyR are required for the maintenance of HSP. Left: PLCβ signaling components depicted in both muscle and neuron at the *Drosophila* NMJ. We detected no apparent role for PLCβ, IP$_3$R, or RyR in baseline neurotransmission. Right: Reduced postsynaptic glutamate receptor function – either due to deletion of the *GluRIIA* gene or expression of *UAS-GluRIII[RNAi]* – drives a chronic form of PHP that is maintained throughout life. A retrograde, muscle-to-nerve signal instructs the neuron to increase the number of neurotransmitter vesicles released (quantal content). Our data support a model in which long-term maintenance of PHP requires PLCβ and its effectors in both the presynaptic neuron and postsynaptic muscle, but these factors are dispensable for the rapid induction of PHP.

**Supplementary Tables S1-S7. Summary Electrophysiological Data.** Genotypes and rearing conditions for electrophysiological data presented in the study (corresponding figures specified). For GAL4 drivers, "*Pre* + *Post-Gal4*" denotes a genetic combination of *elaV(C155)-Gal4/Y; Sca-Gal4/+; BG57-Gal4/+* (see Materials and Methods). Average values ± SEM are presented for each electrophysiological parameter, with $n$ = number of NMJs recorded. Values include miniature excitatory postsynaptic potential (mEPSP) amplitude, mEPSP frequency (Freq), excitatory postsynaptic potential (EPSP) amplitude, quantal content (QC), and QC corrected for non-linear summation (NLS). * $p < 0.05$, ** $p < 0.01$, *** $p < 0.001$ by Student's T-Test vs. unchallenged control.

**Supplementary File. Raw Data Workbook.** Microsoft Excel format. Each tab corresponds to a figure in the paper. Raw data for individual measures in the manuscript. An exception is the screen data for Figure 2. Those data are summarized in Supplementary Table S2. Eelectrophsyiologial measures shown for individual NMJ recordings include the same measures summarized in Tables S1-S7, with the addition of resting membrane potential (RMP), which allows for calculation of QC

1092 corrected for non-linear summation. Synapse growth measures are shown in the tab for Figure 3,
1093 and include bouton counts, muscle area ($\mu m^2$), and boutons per $\mu m^2$.

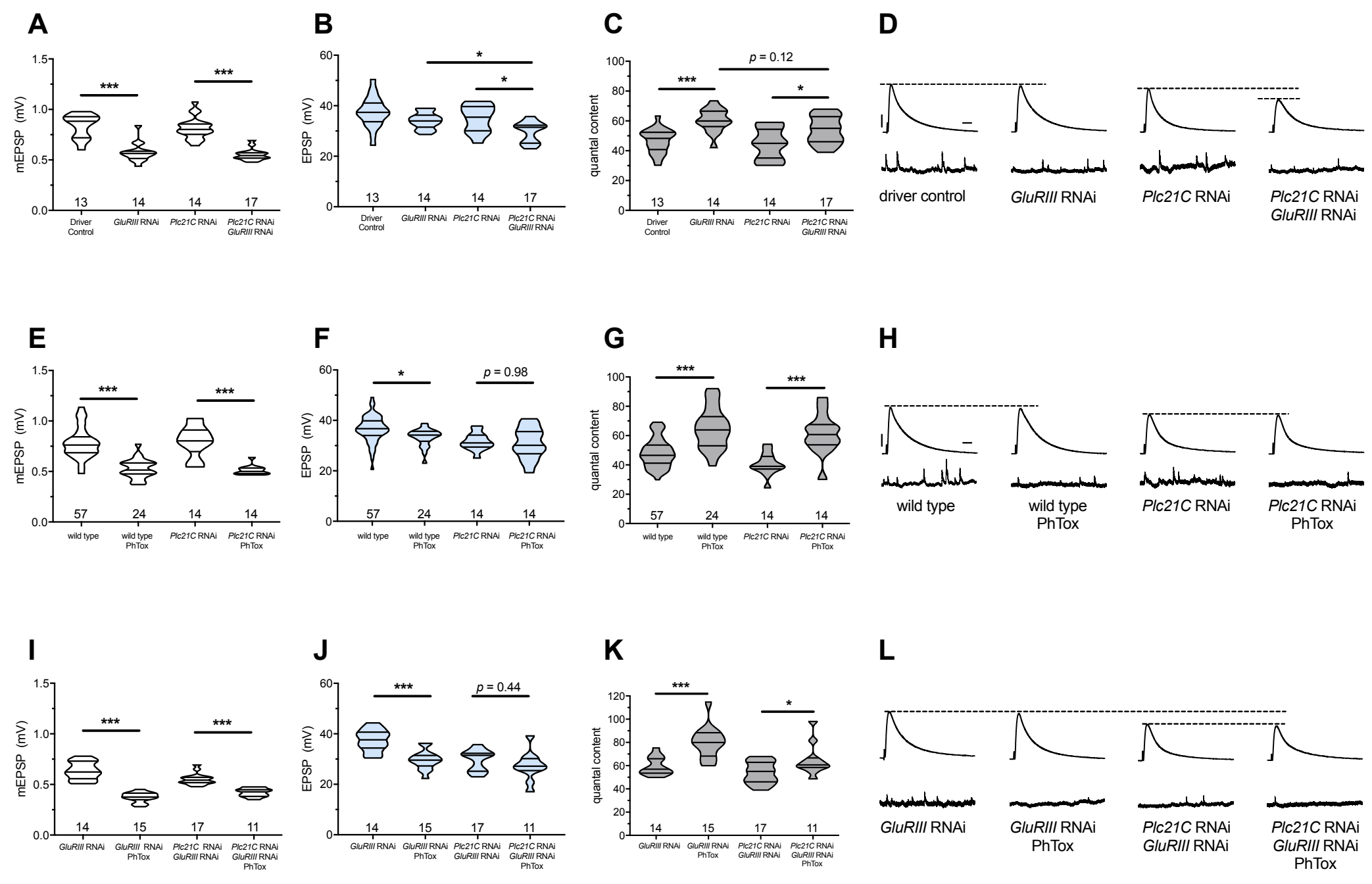
A
mEPSP (mV)
1.5
1.0
0.5
0.0
***
***
13
14
14
17
Driver Control
GluRIII RNAi
Plc21C RNAi
Plc21C RNAi GluRIII RNAi
B
EPSP (mV)
60
40
20
0
*
*
13
14
14
17
Driver Control
GluRIII RNAi
Plc21C RNAi
Plc21C RNAi GluRIII RNAi
C
quantal content
100
80
60
40
20
0
p = 0.12
***
*
13
14
14
17
Driver Control
GluRIII RNAi
Plc21C RNAi
Plc21C RNAi GluRIII RNAi
D
driver control
GluRIII RNAi
Plc21C RNAi
Plc21C RNAi GluRIII RNAi
E
mEPSP (mV)
1.5
1.0
0.5
0.0
***
***
57
24
14
14
wild type
wild type PhTox
Plc21C RNAi
Plc21C RNAi PhTox
F
EPSP (mV)
60
40
20
0
*
p = 0.98
57
24
14
14
wild type
wild type PhTox
Plc21C RNAi
Plc21C RNAi PhTox
G
quantal content
100
80
60
40
20
0
***
***
57
24
14
14
wild type
wild type PhTox
Plc21C RNAi
Plc21C RNAi PhTox
H
wild type
wild type PhTox
Plc21C RNAi
Plc21C RNAi PhTox
I
mEPSP (mV)
1.5
1.0
0.5
0.0
***
***
14
15
17
11
GluRIII RNAi
GluRIII RNAi PhTox
Plc21C RNAi GluRIII RNAi
Plc21C RNAi GluRIII RNAi PhTox
J
EPSP (mV)
60
40
20
0
***
p = 0.44
14
15
17
11
GluRIII RNAi
GluRIII RNAi PhTox
Plc21C RNAi GluRIII RNAi
Plc21C RNAi GluRIII RNAi PhTox
K
quantal content
120
100
80
60
40
20
0
***
*
14
15
17
11
GluRIII RNAi
GluRIII RNAi PhTox
Plc21C RNAi GluRIII RNAi
Plc21C RNAi GluRIII RNAi PhTox
L
GluRIII RNAi
GluRIII RNAi PhTox
Plc21C RNAi GluRIII RNAi
Plc21C RNAi GluRIII RNAi PhTox

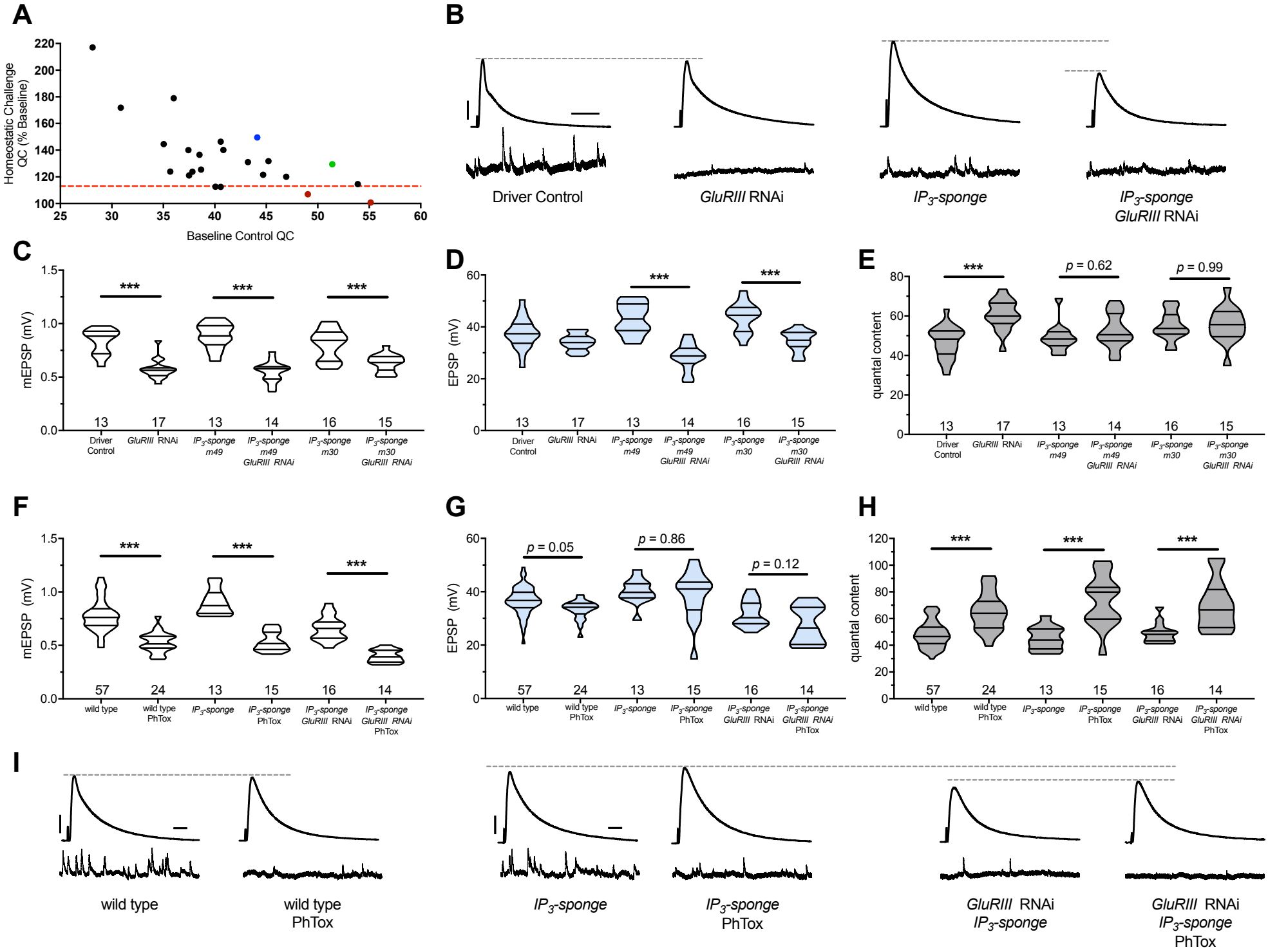
A
Homeostatic Challenge QC (% Baseline)
Baseline Control QC
B
Driver Control
GluRIII RNAi
IP3-sponge
IP3-sponge GluRIII RNAi
C
mEPSP (mV)
Driver Control
GluRIII RNAi
IP3-sponge m49
IP3-sponge m49 GluRIII RNAi
IP3-sponge m30
IP3-sponge m30 GluRIII RNAi
D
EPSP (mV)
E
quantal content
p = 0.62
p = 0.99
F
wild type
wild type PhTox
IP3-sponge
IP3-sponge PhTox
IP3-sponge GluRIII RNAi
IP3-sponge GluRIII RNAi PhTox
G
p = 0.05
p = 0.86
p = 0.12
H
I
wild type
wild type PhTox
IP3-sponge
IP3-sponge PhTox
GluRIII RNAi IP3-sponge
GluRIII RNAi IP3-sponge PhTox

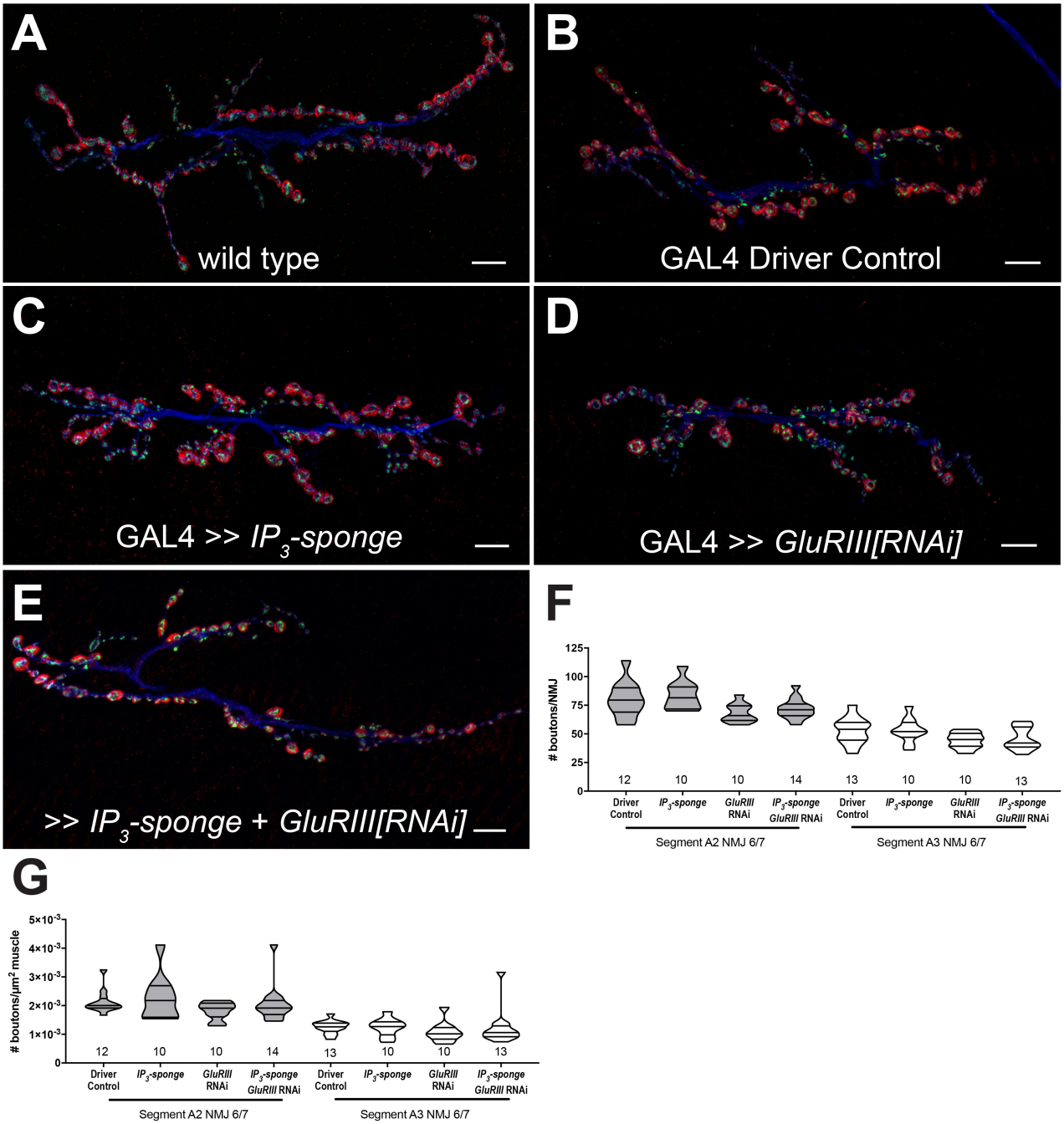
A
wild type
B
GAL4 Driver Control
C
GAL4 >> IP3-sponge
D
GAL4 >> GluRIII[RNAi]
E
>> IP3-sponge + GluRIII[RNAi]
F
# boutons/NMJ
125
100
75
50
25
0
12
10
10
14
13
10
10
13
Driver Control
IP3-sponge
GluRIII RNAi
IP3-sponge GluRIII RNAi
Driver Control
IP3-sponge
GluRIII RNAi
IP3-sponge GluRIII RNAi
Segment A2 NMJ 6/7
Segment A3 NMJ 6/7
G
# boutons/μm2 muscle
5×10-3
4×10-3
3×10-3
2×10-3
1×10-3
0
12
10
10
14
13
10
10
13
Driver Control
IP3-sponge
GluRIII RNAi
IP3-sponge GluRIII RNAi
Driver Control
IP3-sponge
GluRIII RNAi
IP3-sponge GluRIII RNAi
Segment A2 NMJ 6/7
Segment A3 NMJ 6/7

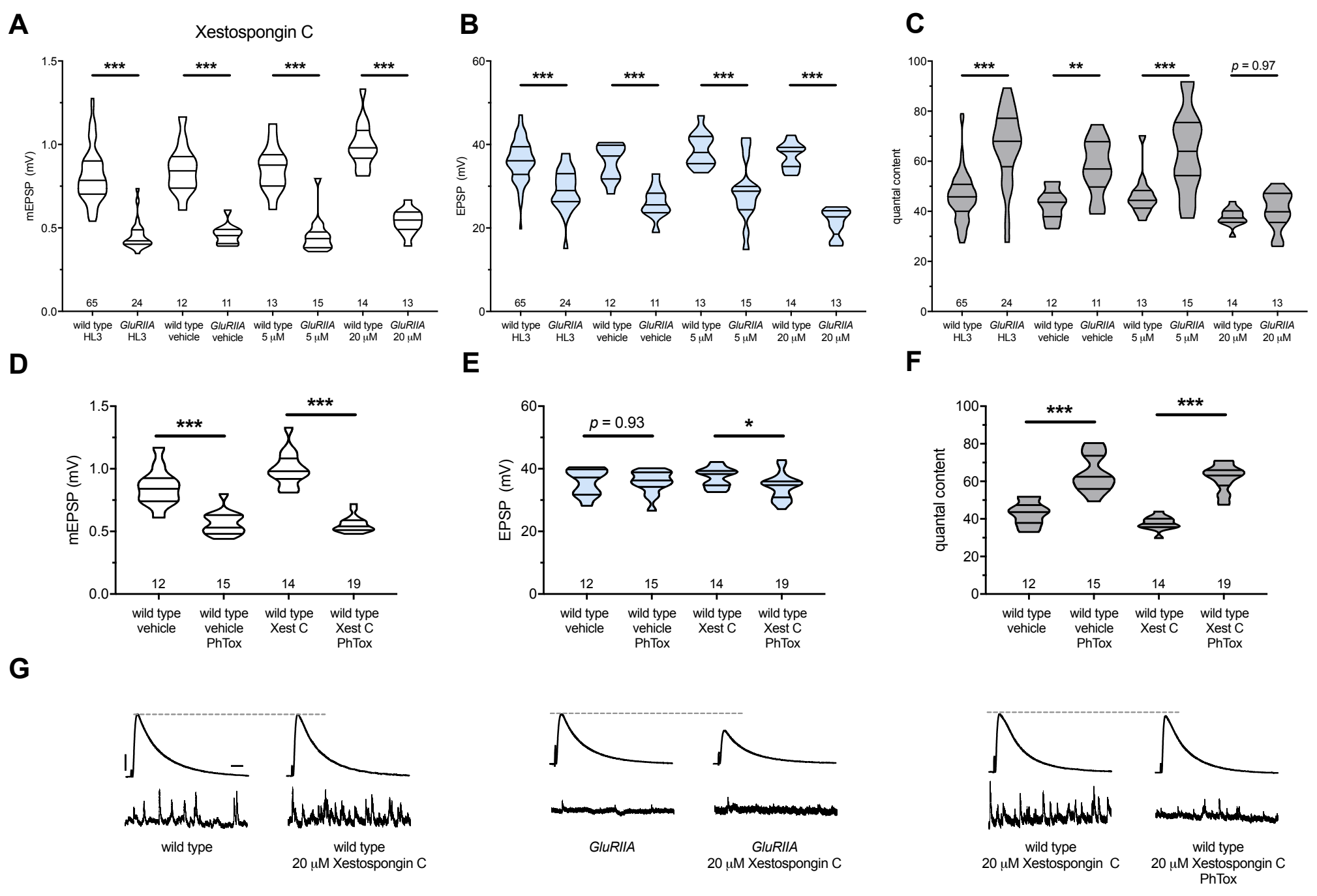
A
Xestospongin C
mEPSP (mV)
1.5
1.0
0.5
0.0
***
65
24
12
11
13
15
14
13
wild type HL3
GluRIIA HL3
wild type vehicle
GluRIIA vehicle
wild type 5 μM
GluRIIA 5 μM
wild type 20 μM
GluRIIA 20 μM
B
EPSP (mV)
60
40
20
0
C
quantal content
100
80
60
40
20
0
**
p = 0.97
D
E
F
wild type vehicle
wild type vehicle PhTox
wild type Xest C
wild type Xest C PhTox
*
G
wild type
wild type 20 μM Xestospongin C
GluRIIA
GluRIIA 20 μM Xestospongin C
wild type 20 μM Xestospongin C
wild type 20 μM Xestospongin C PhTox

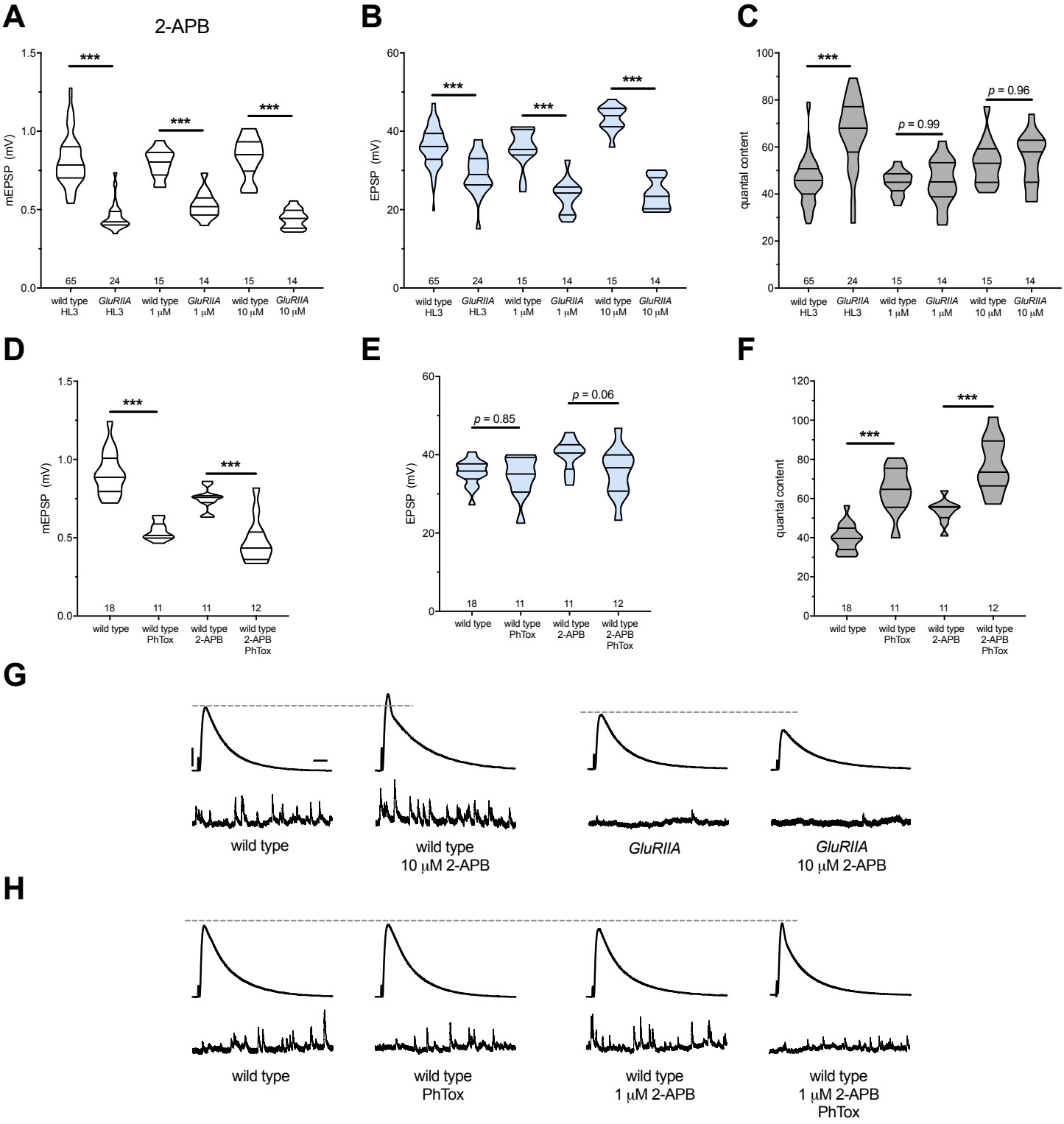
A
2-APB
mEPSP (mV)
1.5
1.0
0.5
0.0
***
***
***
65
24
15
14
15
14
wild type HL3
GluRIIA HL3
wild type 1 μM
GluRIIA 1 μM
wild type 10 μM
GluRIIA 10 μM
B
EPSP (mV)
60
40
20
0
***
***
***
65
24
15
14
15
14
wild type HL3
GluRIIA HL3
wild type 1 μM
GluRIIA 1 μM
wild type 10 μM
GluRIIA 10 μM
C
quantal content
100
80
60
40
20
0
***
p = 0.99
p = 0.96
65
24
15
14
15
14
wild type HL3
GluRIIA HL3
wild type 1 μM
GluRIIA 1 μM
wild type 10 μM
GluRIIA 10 μM
D
mEPSP (mV)
1.5
1.0
0.5
0.0
***
***
18
11
11
12
wild type
wild type PhTox
wild type 2-APB
wild type 2-APB PhTox
E
EPSP (mV)
60
40
20
0
p = 0.85
p = 0.06
18
11
11
12
wild type
wild type PhTox
wild type 2-APB
wild type 2-APB PhTox
F
quantal content
120
100
80
60
40
20
0
***
***
18
11
11
12
wild type
wild type PhTox
wild type 2-APB
wild type 2-APB PhTox
G
wild type
wild type 10 μM 2-APB
GluRIIA
GluRIIA 10 μM 2-APB
H
wild type
wild type PhTox
wild type 1 μM 2-APB
wild type 1 μM 2-APB PhTox

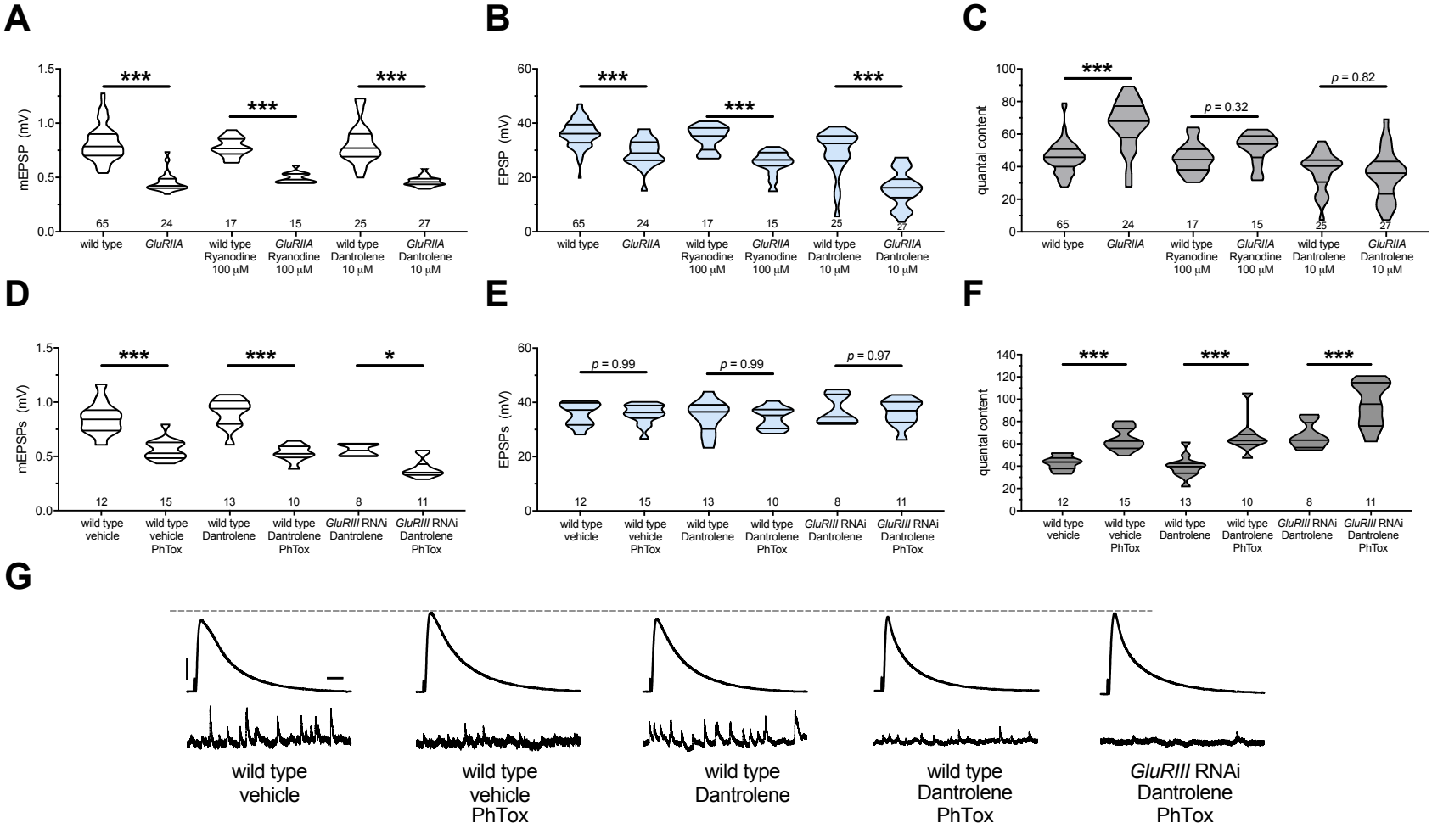
A
mEPSP (mV)
1.5
1.0
0.5
0.0
***
***
***
65
24
17
15
25
27
wild type
GluRIIA
wild type Ryanodine 100 μM
GluRIIA Ryanodine 100 μM
wild type Dantrolene 10 μM
GluRIIA Dantrolene 10 μM
B
EPSP (mV)
60
40
20
0
***
***
***
65
24
17
15
25
27
wild type
GluRIIA
wild type Ryanodine 100 μM
GluRIIA Ryanodine 100 μM
wild type Dantrolene 10 μM
GluRIIA Dantrolene 10 μM
C
quantal content
100
80
60
40
20
0
***
p = 0.32
p = 0.82
65
24
17
15
25
27
wild type
GluRIIA
wild type Ryanodine 100 μM
GluRIIA Ryanodine 100 μM
wild type Dantrolene 10 μM
GluRIIA Dantrolene 10 μM
D
mEPSPs (mV)
1.5
1.0
0.5
0.0
***
***
*
12
15
13
10
8
11
wild type vehicle
wild type vehicle PhTox
wild type Dantrolene
wild type Dantrolene PhTox
GluRIII RNAi Dantrolene
GluRIII RNAi Dantrolene PhTox
E
EPSPs (mV)
60
40
20
0
p = 0.99
p = 0.99
p = 0.97
12
15
13
10
8
11
wild type vehicle
wild type vehicle PhTox
wild type Dantrolene
wild type Dantrolene PhTox
GluRIII RNAi Dantrolene
GluRIII RNAi Dantrolene PhTox
F
quantal content
140
120
100
80
60
40
20
0
***
***
***
12
15
13
10
8
11
wild type vehicle
wild type vehicle PhTox
wild type Dantrolene
wild type Dantrolene PhTox
GluRIII RNAi Dantrolene
GluRIII RNAi Dantrolene PhTox
G
wild type vehicle
wild type vehicle PhTox
wild type Dantrolene
wild type Dantrolene PhTox
GluRIII RNAi Dantrolene PhTox

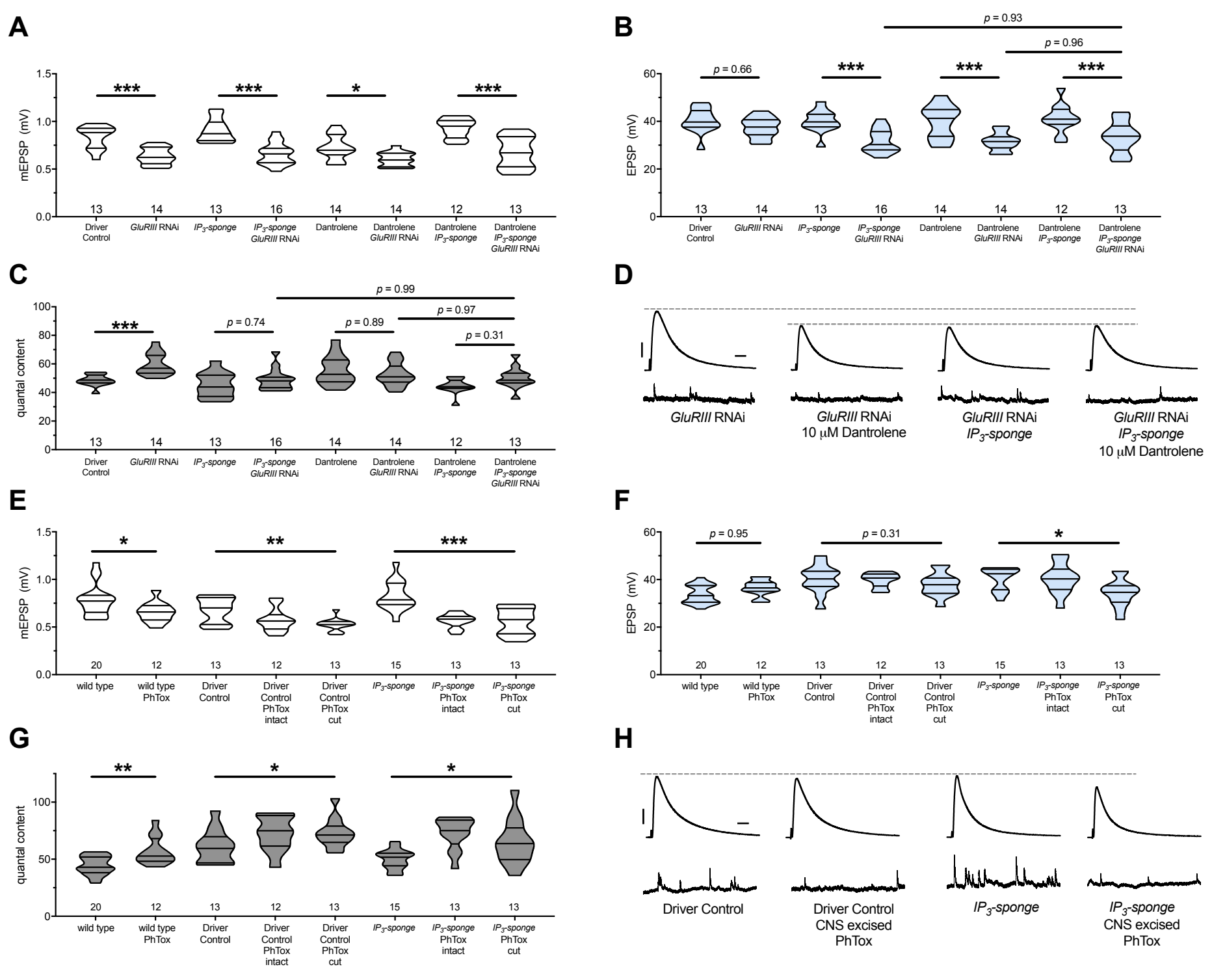
A
mEPSP (mV)
1.5
1.0
0.5
0.0
***
***
*
***
13
14
13
16
14
14
12
13
Driver Control
GluRIII RNAi
IP3-sponge
IP3-sponge GluRIII RNAi
Dantrolene
Dantrolene GluRIII RNAi
Dantrolene IP3-sponge
Dantrolene IP3-sponge GluRIII RNAi
B
EPSP (mV)
60
40
20
0
p = 0.93
p = 0.96
p = 0.66
***
***
***
13
14
13
16
14
14
12
13
Driver Control
GluRIII RNAi
IP3-sponge
IP3-sponge GluRIII RNAi
Dantrolene
Dantrolene GluRIII RNAi
Dantrolene IP3-sponge
Dantrolene IP3-sponge GluRIII RNAi
C
quantal content
100
80
60
40
20
0
p = 0.99
p = 0.97
***
p = 0.74
p = 0.89
p = 0.31
13
14
13
16
14
14
12
13
Driver Control
GluRIII RNAi
IP3-sponge
IP3-sponge GluRIII RNAi
Dantrolene
Dantrolene GluRIII RNAi
Dantrolene IP3-sponge
Dantrolene IP3-sponge GluRIII RNAi
D
GluRIII RNAi
GluRIII RNAi
10 μM Dantrolene
GluRIII RNAi
IP3-sponge
GluRIII RNAi
IP3-sponge
10 μM Dantrolene
E
mEPSP (mV)
1.5
1.0
0.5
0.0
*
**
***
20
12
13
12
13
15
13
13
wild type
wild type PhTox
Driver Control
Driver Control PhTox intact
Driver Control PhTox cut
IP3-sponge
IP3-sponge PhTox intact
IP3-sponge PhTox cut
F
EPSP (mV)
60
40
20
0
p = 0.95
p = 0.31
*
20
12
13
12
13
15
13
13
wild type
wild type PhTox
Driver Control
Driver Control PhTox intact
Driver Control PhTox cut
IP3-sponge
IP3-sponge PhTox intact
IP3-sponge PhTox cut
G
quantal content
100
50
0
**
*
*
20
12
13
12
13
15
13
13
wild type
wild type PhTox
Driver Control
Driver Control PhTox intact
Driver Control PhTox cut
IP3-sponge
IP3-sponge PhTox intact
IP3-sponge PhTox cut
H
Driver Control
Driver Control CNS excised PhTox
IP3-sponge
IP3-sponge CNS excised PhTox

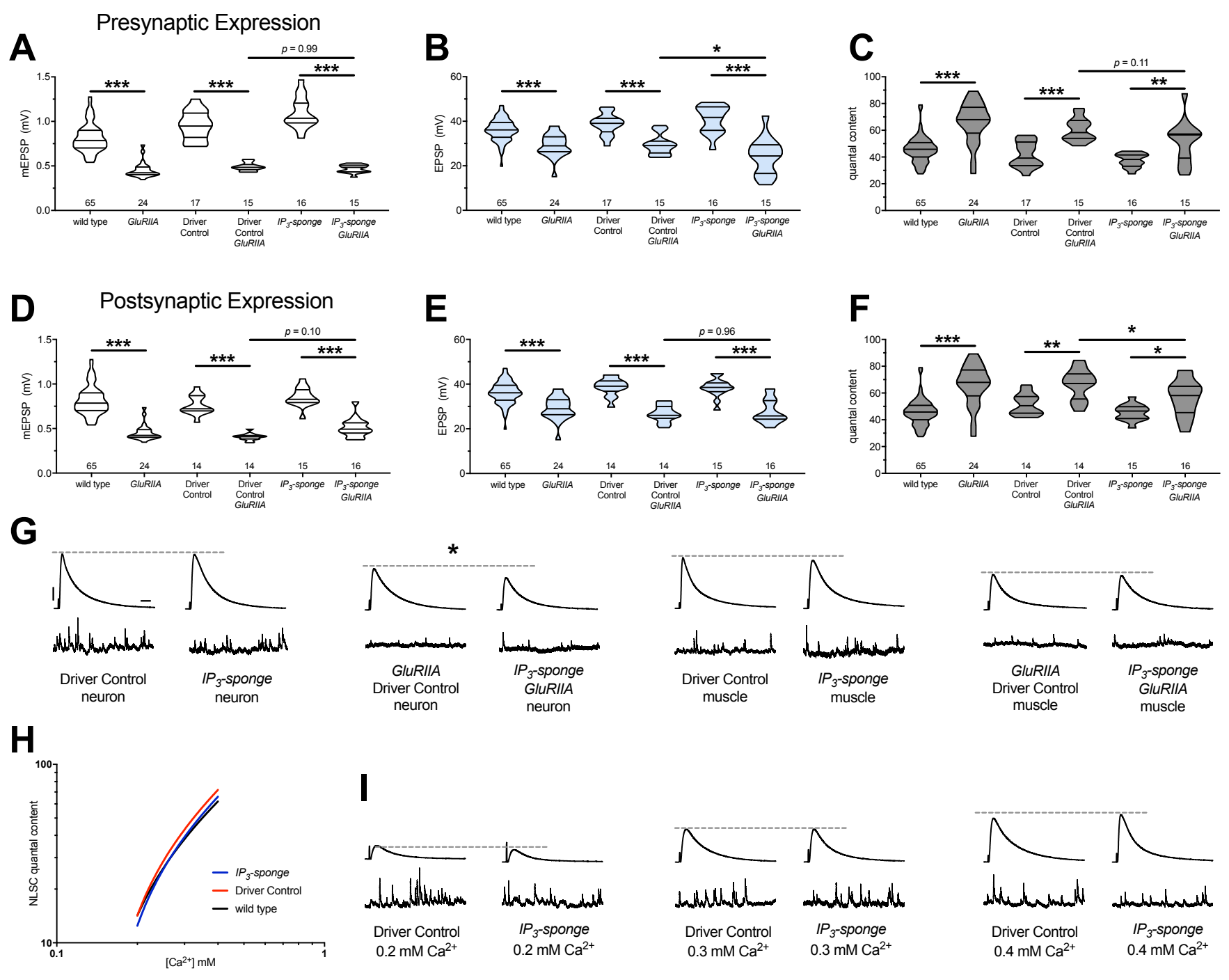
Presynaptic Expression
A
B
C
mEPSP (mV)
EPSP (mV)
quantal content
p = 0.99
p = 0.11
65
24
17
15
16
15
wild type
GluRIIA
Driver Control
Driver Control GluRIIA
IP3-sponge
IP3-sponge GluRIIA
Postsynaptic Expression
D
E
F
p = 0.10
p = 0.96
14
G
Driver Control neuron
IP3-sponge neuron
GluRIIA Driver Control neuron
IP3-sponge GluRIIA neuron
Driver Control muscle
IP3-sponge muscle
GluRIIA Driver Control muscle
IP3-sponge GluRIIA muscle
H
NLSC quantal content
[Ca2+] mM
IP3-sponge
Driver Control
wild type
I
Driver Control 0.2 mM Ca2+
IP3-sponge 0.2 mM Ca2+
Driver Control 0.3 mM Ca2+
IP3-sponge 0.3 mM Ca2+
Driver Control 0.4 mM Ca2+
IP3-sponge 0.4 mM Ca2+

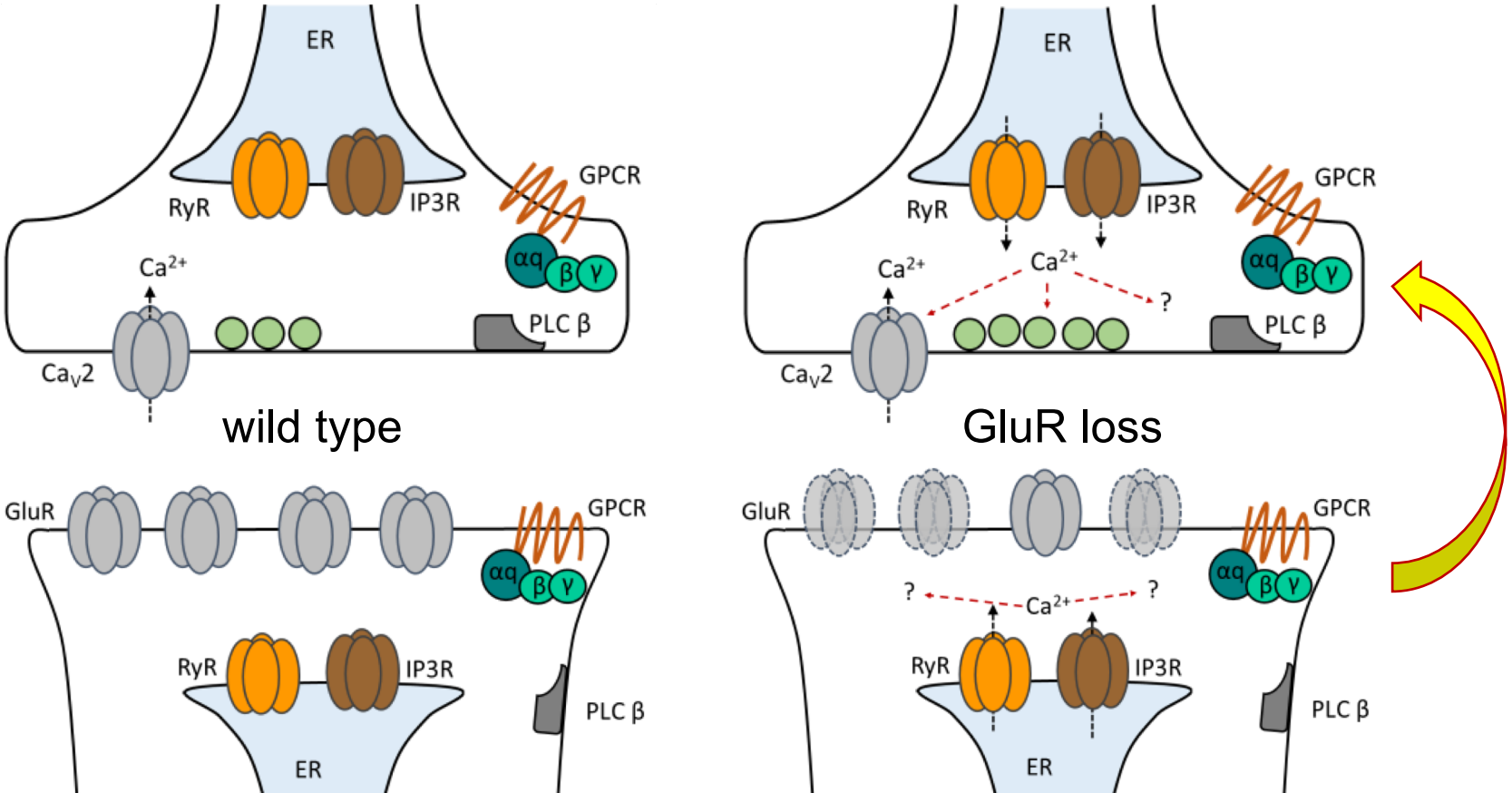
ER
RyR
IP3R
GPCR
αq
β
γ
Ca2+
PLC β
CaV2
wild type
GluR loss
?
GluR